Robust and irreversible impacts of an AMOC collapse on tropical monsoon systems: a multi-model comparison

Maya Ben-Yami[1], Peter Good[2], Laura C Jackson[2], Michel Crucifix[3], Aixue Hu[4], Oleg A. Saenko[5], Didier Swingedouw[6], and Niklas Boers[7]

[1]Technical University of Munich
[2]Met Office
[3]Universite catholique de Louvain
[4]National Center for Atmospheric Research (UCAR)
[5]University of Victoria
[6]French National Centre for Scientific Research (CNRS)
[7]École Normale Supérieure

September 11, 2023

Abstract

A collapse of the Atlantic Meridional Overturning Circulation (AMOC) would have substantial impacts on global precipitation patterns, especially in the vulnerable tropical monsoon regions. We assess these impacts using four state-of-the-art climate models with bistable AMOC. Spatial and seasonal patterns of precipitation change are remarkably consistent across models. We focus on the South American Monsoon (SAM), the West African Monsoon (WAM), the Indian Summer Monsoon (ISM) and the East Asian Summer Monsoon (EASM). Models consistently suggest substantial disruptions for WAM, ISM and EASM with shorter wet and longer dry seasons (-29.07\%,-18.76\% and -3.78\% ensemble mean annual rainfall change, respectively). Models also agree on changes for the SAM, suggesting rainfall increases overall, in contrast to previous studies. These are more pronounced in the southern Amazon (+43.79\%), accompanied by decreasing dry-season length. Consistently across models, our results suggest major rearranging of all tropical monsoon systems in response to an AMOC collapse.

Robust and irreversible impacts of an AMOC collapse on tropical monsoon systems: a multi-model comparison

M. Ben-Yami[1,2], P. Good[3], L. C. Jackson [3], M. Crucifix [4], A. Hu [5], O. Saenko [6], D. Swingedouw [7] and N. Boers [1,2,8]

[1]Earth System Modelling, School of Engineering and Design, Technical University of Munich, Munich, Germany
[2]Potsdam Institute for Climate Impact Research, Potsdam, Germany
[3]Met Office, Exeter, UK
[4]Earth and Life Institute, UCLouvain, Place Louis Pasteur 3, Louvain-La-Neuve, 1348, Belgium
[5]Climate and Global Dynamics Lab, National Center for Atmospheric Research, Boulder, CO 80307, USA
[6]SEOS, University of Victoria, BC, Canada
[7]Environnements et Paléoenvironnements Océaniques et Continentaux (EPOC)— Université de Bordeaux, Pessac, France
[8]Department of Mathematics and Global Systems Institute , University of Exeter, Exeter, UK

Key Points:

- A collapse of the AMOC would cause a major rearrangement of all tropical monsoon systems
- Four state-of-the-art climate models show remarkable agreement on the effects of an AMOC collapse
- These impacts are practically irreversible

Corresponding author: M. Ben-Yami, maya.ben-yami@tum.de

Abstract

A collapse of the Atlantic Meridional Overturning Circulation (AMOC) would have substantial impacts on global precipitation patterns, especially in the vulnerable tropical monsoon regions. We assess these impacts using four state-of-the-art climate models with bistable AMOC. Spatial and seasonal patterns of precipitation change are remarkably consistent across models. We focus on the South American Monsoon (SAM), the West African Monsoon (WAM), the Indian Summer Monsoon (ISM) and the East Asian Summer Monsoon (EASM). Models consistently suggest substantial disruptions for WAM, ISM and EASM with shorter wet and longer dry seasons (-29.07%,-18.76% and -3.78% ensemble mean annual rainfall change, respectively). Models also agree on changes for the SAM, suggesting rainfall increases overall, in contrast to previous studies. These are more pronounced in the southern Amazon (+43.79%), accompanied by decreasing dry-season length. Consistently across models, our results suggest major rearranging of all tropical monsoon systems in response to an AMOC collapse.

Plain Language Summary

The Atlantic Meridional Overturning Circulation (AMOC) is a key element of the Earth's climate system, transporting large amounts of heat and salt northward in the upper layers of the Atlantic ocean. Although its likelihood remains highly uncertain, a collapse of the AMOC in response to anthropogenic climate change would have catastrophic ecological and societal consequences. This is especially true in the vulnerable monsoon regions of the tropics. Yet, the precise effects of an AMOC collapse on the tropical monsoon systems remain unclear. We take advantage of a climate model intercomparison project, and provide a detailed and systematic analysis of the irreversible seasonal impacts of an AMOC collapse on the major tropical monsoon systems. We find remarkable, previously unseen, agreement between four independent state-of-the-art climate models. Consistently across models, our results suggest major rearranging of all tropical monsoon systems in response to an AMOC collapse.

1 Introduction

The Atlantic Meridional Overturning Circulation (AMOC) is a key element of the Earth's climate system, transporting large amounts of heat and salt northward in the upper layers of the Atlantic ocean. Paleoclimate proxy evidence as well as theoretical considerations suggest that the AMOC is bistable, with a second, substantially weaker circulation mode in addition to the present strong mode (Henry et al., 2016; Stommel, 1961; Rahmstorf, 2002). The question whether the AMOC is bistable in comprehensive climate models has been intensely debated in recent years and a rising number of such models exhibit a bistable AMOC (Y. Liu et al., 2014; W. Liu et al., 2017; Jackson & Wood, 2018; Romanou et al., 2023). Concerns have been raised that the AMOC might collapse to its weak state in response to enhanced freshwater inflow into the North Atlantic due anthropogenic warming and resulting Greenland ice sheet melting (W. Liu et al., 2017), although the 6th assessment report (AR6) of the International Panel on Climate Change (IPCC) concludes that such a collapse has moderate likelihood to happen before 2100 (Arias et al., 2021). Studying a potential AMOC collapse is however of great interest given the severe global impacts it would have. There are several lines of proxy-based evidence suggesting that the AMOC has indeed weakened in the last decades to centuries (Caesar et al., 2021) and comprehensive models predict that it will weaken further under anthropogenic global warming (Lee et al., 2021). In addition, evidence that the recent AMOC weakening might be associated with a decrease of stability of the current circulation mode has been identified in sea-surface temperature (SST) and salinity based fingerprints of the AMOC strength (Boers, 2021).

If the AMOC were to collapse, the reduced northward heat transport would cause a relative cooling of the northern hemisphere, and the change in inter-hemispheric energy transport would lead to a shift of the thermal equator and hence a southward shift of the inter-tropical convergence zone (ITCZ) (Jackson et al., 2015). The subsequent global-scale reorganization of the atmospheric circulation would have far-reaching effects in the Pacific as well as in the Atlantic (Orihuela-Pinto et al., 2022). As the ITCZ is the main source of tropical rainfall, an AMOC collapse and associated southward ITCZ shift would likely have substantial consequences for the tropical monsoon systems. Given their socioeconomic and ecological importance, a detailed analysis of the impacts of an AMOC collapse on these monsoon systems is needed. Over half of the world's population live in climates dominated by tropical monsoons (Moon & Ha, 2020; Wang et al., 2021). Most of these are in developing countries, where land use is dominated by agriculture, so depends heavily on the rain the monsoons bring. These regions are thus vulnerable to any changes in the characteristics of the monsoon rains, whether they are changes in the timing or the amount of rainfall (WRCP, n.d.). This makes tropical monsoon regions a high priority regarding possible impacts of anthropogenic global warming (Wang et al., 2021).

There exist multiple lines of proxy evidence to assess the impacts of an AMOC collapse on the tropical monsoon systems during past climate conditions (Sun et al., 2012; Sandeep et al., 2020; Häggi et al., 2017; Mosblech et al., 2012; Wassenburg et al., 2021; Marzin et al., 2013). To study the effects in more detail and for present-day climate conditions, so-called hosing experiments in general circulation models (GCMs) are used, in which freshwater is added to a region of the north Atlantic for a long period of time, forcing the AMOC to weaken and potentially collapse to a weaker state. Some studies have also focused on individual monsoon systems such as the South American Monsoon (SAM) (Good et al., 2021; Parsons et al., 2014), the West African Monsoon (WAM) (Chang et al., 2008), the Indian Summer Monsoon (ISM) (Sandeep et al., 2020; Marzin et al., 2013) and the East Asian Summer Monsoon (EASM) (Yu et al., 2009). Most studies find an overall decrease in annual mean precipitation of the different monsoon systems. For tropical South America, however, older simulations suggesting increased annual rainfall sums (Stouffer et al., 2006) are in contrast with more recent modelling studies suggesting decreases (Jackson et al., 2015). In addition, both Parsons et al. (2014) and Good et al. (2021) note that it is important to analyse the atmospheric response throughout the seasonal cycle. Specifically, Parsons et al. (2014) find that a wetter dry season after an AMOC collapse increased the overall Amazon vegetation productivity. The overall sign of the precipitation change over tropical South America in response to an AMOC collapse remains debated. This debate is complicated by the fact that there has been no cross-model AMOC hosing comparison since (Stouffer et al., 2006), and in general it is difficult to compare the impacts in experiments with different hosing scenarios.

The bi-stability of the AMOC has long been supported by theory, simple and intermediate-complexity models (Stommel, 1961; Rahmstrof et al., 2005), as well as the paleoclimate data record (Rahmstorf, 2002; Henry et al., 2016). Nevertheless, many GCMs do not exhibit the hysteresis associated with bi-stability (Y. Liu et al., 2014; Drijfhout et al., 2011), although more recent studies do find a persistent weak state (Jackson & Wood, 2018; Romanou et al., 2023). The North Atlantic Hosing Model Intercomparison Project (NAHosMIP) compares eight different models from the sixth phase of the Climate Model Intercomparison Project (CMIP6), aiming to investigate AMOC response and associated hysteresis (Jackson et al., 2022). Four out of the eight studied models exhibit a bistable AMOC, and this allows for a unique opportunity to investigate the effects of an AMOC collapse across models. Not only do all four models use the same hosing scenario, but the bistability of their AMOC allows us to investigate the permanent and practically irreversible impacts of the stable weak AMOC state that occurs after the hosing has been stopped. This is in contrast to most AMOC hosing studies, in which the hosing is continuously applied during the study period.

The different models of NAHosMIP exhibit a range of different patterns and biases, and thus comparing the effect of an AMOC collapse across models allows us to make robust statements on its effect on tropical precipitation. In this study we use results from the four models in NAHosMIP that remain in the weak state after the hosing is stopped: HadGEM3-GC3-1MM, CanESM5, CESM2 and IPSL-CM6A-LR (hereafter abbreviated as HadGEM, CanESM, CESM and IPSL). We compare spatial precipitation fields from the the control runs of these models (piControl) to scenarios in which a constant 0.3 Sv of hosing is applied over the North Atlantic for 50 years (100 years for the IPSL model), thus weakening the AMOC. After the hosing is stopped the AMOC remains in the weak state (see Methods for more details).

2 Results

2.1 Global change in precipitation

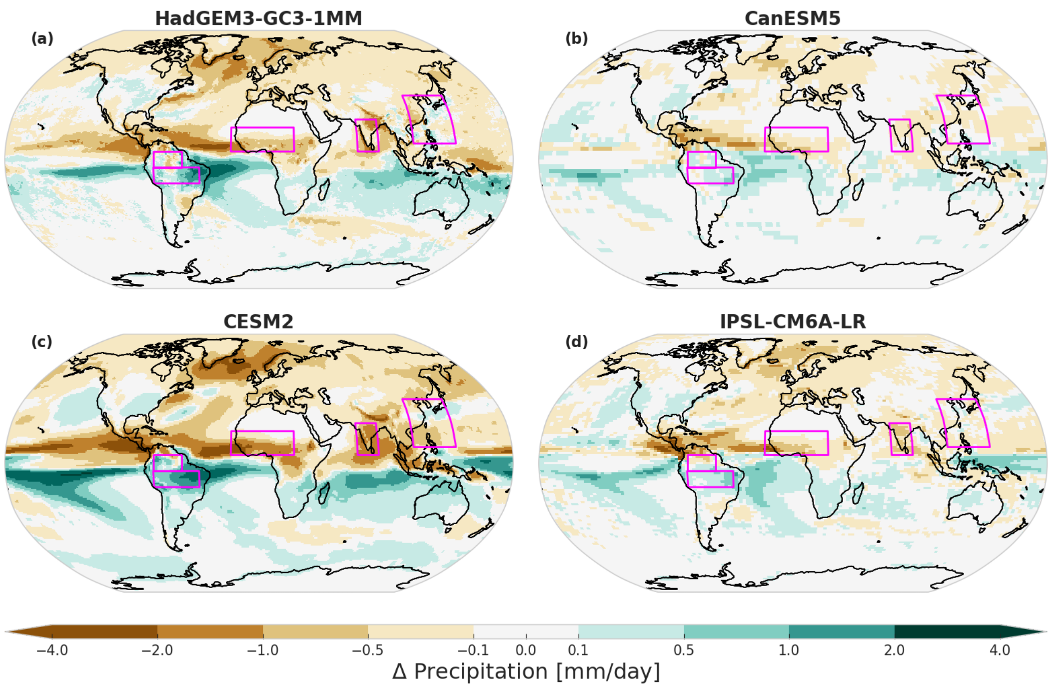

Figure 1. Modelled impacts of an AMOC collapse on global precipitation. Average precipitation shifts (weak AMOC run minus piControl run) for a. HadGEM3, b. CanESM, c. CESM, and d. IPSL. Note the southward ITCZ shift and the general pattern of Northern-Hemisphere drying and Southern-Hemisphere wettening in response to an AMOC collapse, shared by all models. The magenta boxes show the monsoon regions investigated in this work: the two parts of the SAM as well as the WAM, ISM, and EASM (see Methods and Table S1).

The model control runs have biases when compared to observations (see Figure S1). To understand the effect of an AMOC collapse on global precipitation, it is therefore more informative to analyse the differences between the post- and pre-hosing model runs than between the post-hosing runs and observations. In the following we will in general refer to the post-hosing collapsed state as the weak AMOC. The resulting pattern of global precipitation shifts in response to an AMOC collapse is then remarkably similar in all four models (Figures 1(a)-(d) and S2): (i) a southward shift of the ITCZ and overall increased (decreased) precipitation over the southern (northern) hemisphere; (ii) a general reduction of precipitation of the higher latitudes; (iii) reduced precipitation in all monsoon regions except the SAM; and (iv) increased precipitation over most of the Amazon, especially in the east.

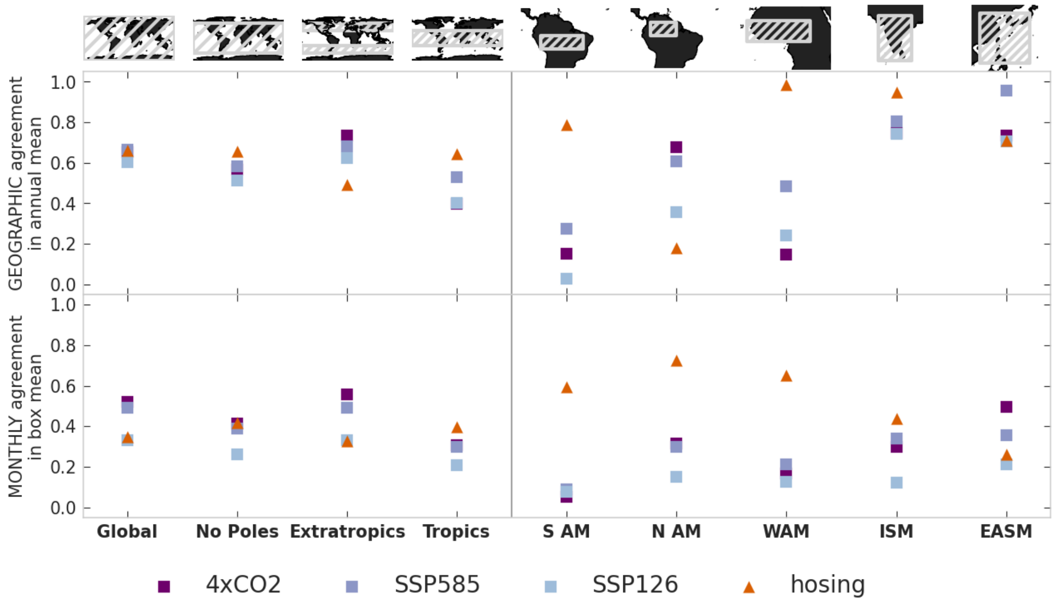

Figure 2. Model agreement in the NAHosMIP experiments compared to the agreement in CMIP6 warming experiments. (a) The fraction of gridcells in a given geographic region that agree on the sign of change in the annual mean rainfall. (b) The fraction of months in a year that agree on the sign of change in the mean monthly rainfall in the given box. The square markers show the agreement for the 4xCO2 (purple), SSP585 (lilac) and SSP126 (light blue) experiments. The triangular orange marker shows the agreement of the hosing experiments. The regions of analysis are defined in Tables S1 and S2, and are shown as grey dashed boxes on the maps in the top row. A horizontal grey line separates the values for the global boxes from the regional monsoon boxes. The exact values are given in Tables S2 and S3.

The four models show a remarkable agreement on the sign of precipitation changes in the tropics (20°S-20°N) in response to an AMOC collapse. The fraction of land in which the sign of change is consistent in the four models is 0.64 in the tropics, and is as large as 0.99 in some of the individual monsoon regions (see Table S2 and Figure 2). The agreement in the seasonal cycle change is also especially high in the Atlantic monsoon regions (Table S3). Notably, in the tropics the agreement between these four models on the impacts of an AMOC collapse are consistently higher than the agreement found in different CMIP6 warming experiments (Figure 2). As CMIP6 models are known to have inconsistent precipitation predictions in the tropics (Lee et al., 2021; Moon & Ha, 2020; Wang et al., 2021), the higher agreement found in the hosing experiments is even more remarkable.

Whilst the overall pattern of change in the four models subsequent to an AMOC collapse is in agreement, the magnitude of the precipitation change varies. CanESM and IPSL have a comparably small change in precipitation following an AMOC collapse, of the order of 0.5 mm/day in the monsoon regions (Figure 1). The model with the largest precipitation change is CESM, with a precipitation change over the SAM, ISM and WAM in CESM of the order of 2-3 mm/day, with a slightly smaller change in the EASM. HadGEM

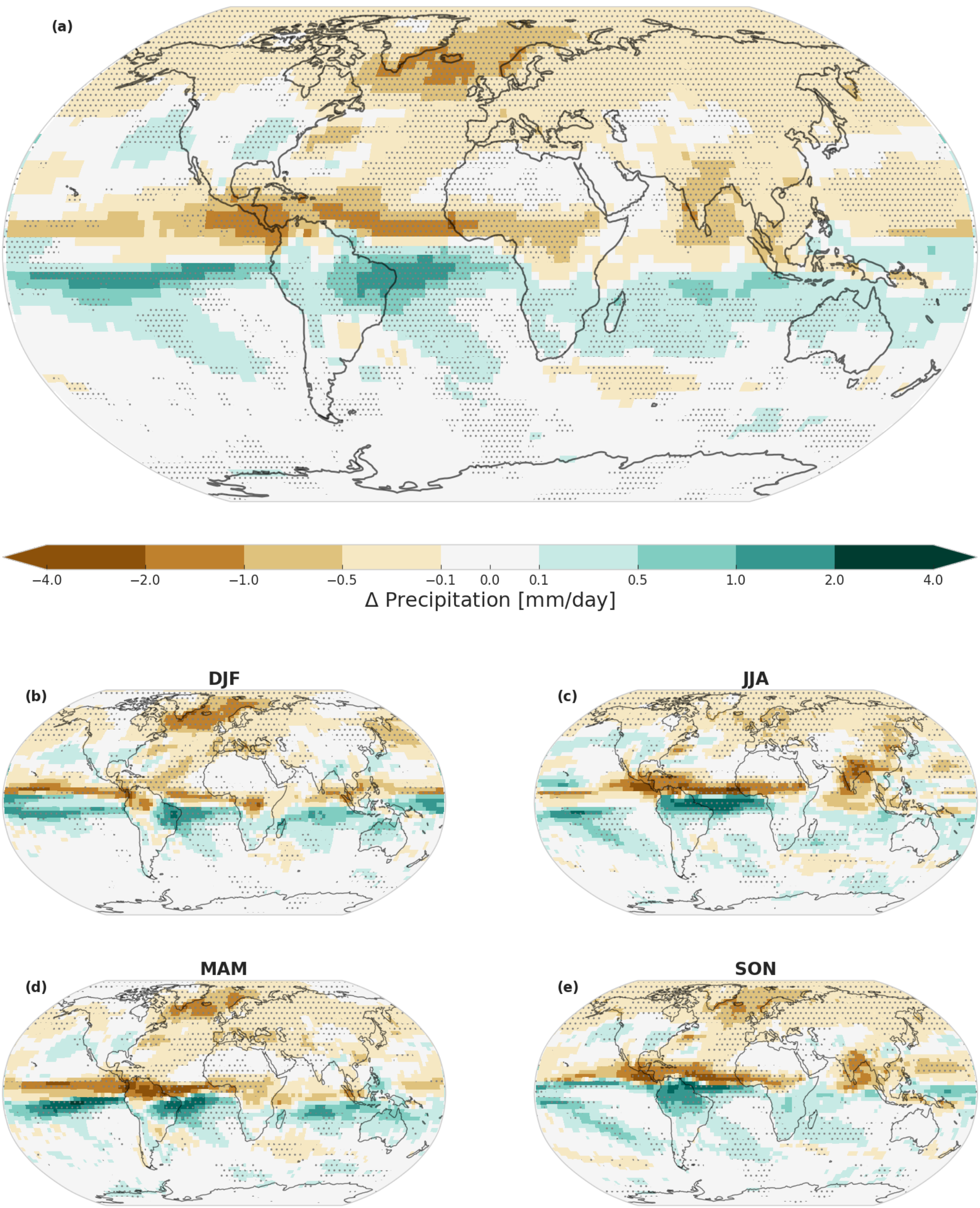

Figure 3. Average precipitation anomaly (weak AMOC run minus piControl run) for the ensemble mean of the four models. Figure (a) shows the annual mean, whilst Figures (b)-(e) show the season anomalies in DJF, JJA, MAM and SON, respectively. The stippling in each Figure indicates regions in which all four model anomalies agree in sign for that mean.

is midway between the two extremes with changes on the order of 1 mm/day. HadGEM also has a more complex precipitation change pattern for the SAM, with less rainfall over about half of the northern Amazon region and more rainfall over the rest of the region.

Even in light of the differences in magnitude, the agreement between the models is remarkable, given that previous generations of models have shown considerably stronger differences and inconsistencies (for example, Jackson et al. (2015) showed a drying over almost all of the Amazon, in contrast to the multi-model comparison in (Stouffer et al., 2006)). This similarity in our models justifies a calculation of the ensemble mean precipitation anomaly (Figure 3). The ensemble mean shows the same pattern as described above, with a drying of all monsoon regions except the SAM. The ensemble mean percentage changes in rainfall in the monsoon regions are (Figure S2): +5.2% in the Northern Amazon, +43.79% in the Southern Amazon, -29.07% in the WAM, -18.76% in the ISM and -3.78% in the EASM.

To understand the different magnitudes of model responses to an AMOC collapse we analyse the seasonal cycle of the Atlantic ITCZ following (Good et al., 2021) (see Methods). A smaller shift of the Atlantic ITCZ after an AMOC collapse should result in a smaller precipitation anomaly, and this is reflected in the respective Atlantic ITCZ shifts of the models (Figure S3 (a)-(d)). IPSL and CanESM have only a small ($\leq 1°$) latitudinal shift in the Atlantic ITCZ between the control and weak AMOC, whilst the shift in HadGEM and CESM is a few times larger. The latter two also have a seasonal Atlantic ITCZ cycle which is closer to the observations (see Methods for details). The ordering of magnitudes is also mirrored in the amount the model AMOC weakens from the piControl to the weak state in the respective models (Figure S4).

2.2 Changes in the seasonal cycle

Whilst the pattern of annual mean rainfall anomaly is informative for understanding the global effect of an AMOC collapse, the effect on the major tropical monsoon systems is by definition highly seasonally dependent. We investigate the seasonal change in rainfall in two ways. First, calculating the average seasonal cycle in the whole of a given monsoon region, and second, calculating the geographic pattern of change in dry and wet seasons in these regions.

All piControl model runs match the overall pattern of the observed seasonal rainfall, but there are considerable biases in some cases (Figure 4). Their strengths depend on the region and model, with no model standing out as the best one in matching the observations across regions. For example, the best match between observations and control runs for the WAM and ISM is in CESM, but CanESM reproduces the southern Amazon rainfall better. CanESM, on the other hand, has the largest biases of any model in the northern Amazon and the ISM, with a difference of over 6 mm/day in the ISM wet season.

As discussed above, the sign of this monthly precipitation change is overall in agreement between models (Figures 2b and S5b and Table S3). In general there is high agreement in the hosing experiments for the SAM and WAM and slightly less for the ISM and EASM, which is likely due to the former being directly impacted by the southward shift of the Atlantic ITCZ.

The pattern of seasonal cycle change present in these models is: (i) The southern Amazon gains a small amount of precipitation in all months, with the exception of CanESM showing a small precipitation decrease in the January-to-March part of the wet season (Figure 4a). The overall gains are in line with a southward shift of the Atlantic ITCZ, since this box extends from 5° S down to 15° S, that is, on the edge of the Atlantic ITCZ extent. A southward shift of the Atlantic ITCZ therefore brings more of the austral summer precipitation into this area; (ii) The northern Amazon has the most complex pat-

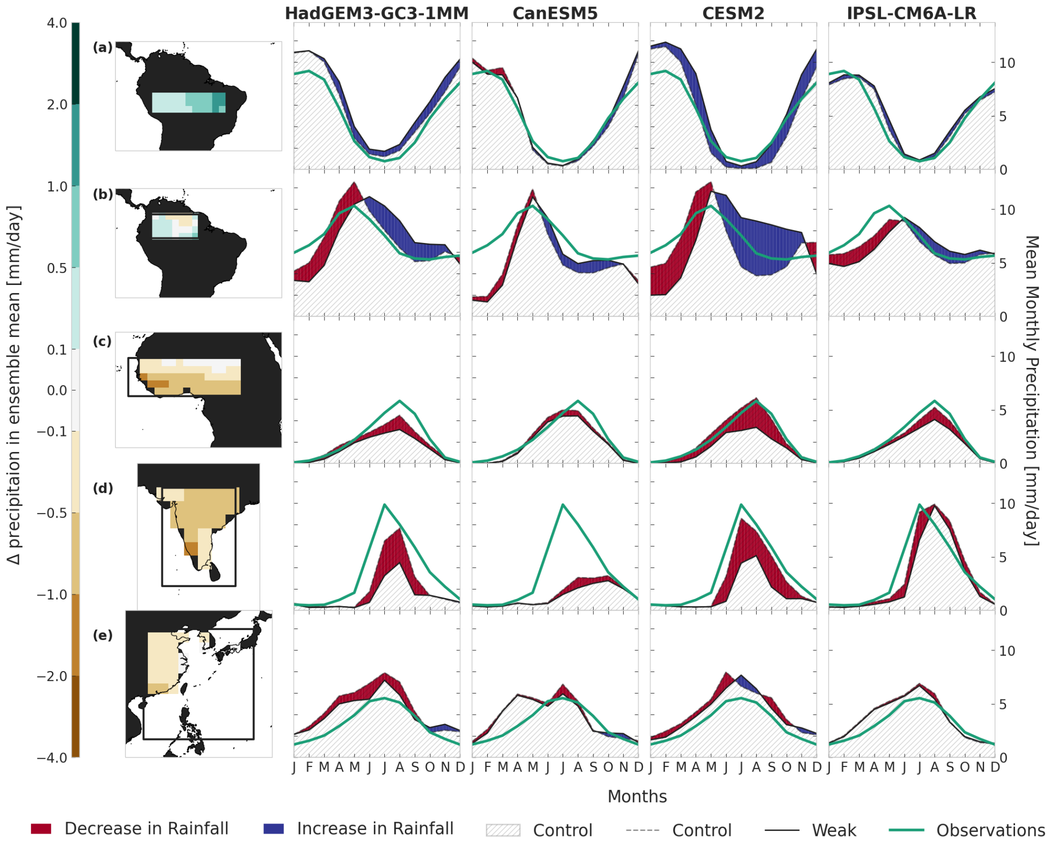

Figure 4. Changes in the seasonal cycle due to an AMOC collapse in two parts of the SAM (a,b), as well as in the WAM (c), ISM (d), and EASM (e). The first column shows the ensemble mean average yearly precipitation change in the given region (i.e., average over all four models). Taking this ensemble mean is justified by the high model agreement as identified above. The remaining columns show the change in precipitation from the average seasonal cycle in the pi-Control (dot-dashed line) to the weak AMOC run (solid line) for the four different models. The area under the graph is shaded in red where the rainfall decreases and in blue where it increases in response to an AMOC collapse. The area common to both is marked by black hatches. The observed seasonal cycle in shown as the turquoise line. Coordinates for the monsoon boxes can be found in Table S1.

tern, with reduced rainfall in the piControl wet season and increased rainfall in the pi-Control dry season (Figure 4b). This is due to a combined shift in time of the wet season to later in the year and a reduction in the overall rainfall. It should be noted that this region also has a complex spatial pattern of changing rainfall in addition to the seasonal pattern (see Figures 1, 3 and 5); (iii) The WAM has a clear pattern (Figure 4c), showing decrease in rainfall during the wet season in all models. In CESM this is a 50% rainfall decrease, and in the other models closer to 5-10%. Since the WAM is at the northern edge of the Atlantic ITCZ range, such a drying is to be expected from a southward shift of the ITCZ; (iv) The ISM has a similar pattern to the WAM, with a substantial loss of rainfall during the wet season (Figure 4d); and (v) The EASM shows a general drying which is relatively small in all models. All models also show a small increase in dry-season rainfall, but both these changes are too small to change the amplitude, timing or structure of the overall seasonal cycle. CESM also shows a shift of the peak wet season rainfall from June to August (Figure 4e).

The magnitudes of all these changes in the different models are in line with the shift in the Atlantic ITCZ - the larger the shift, the larger the precipitation change, independently of the piControl model bias.

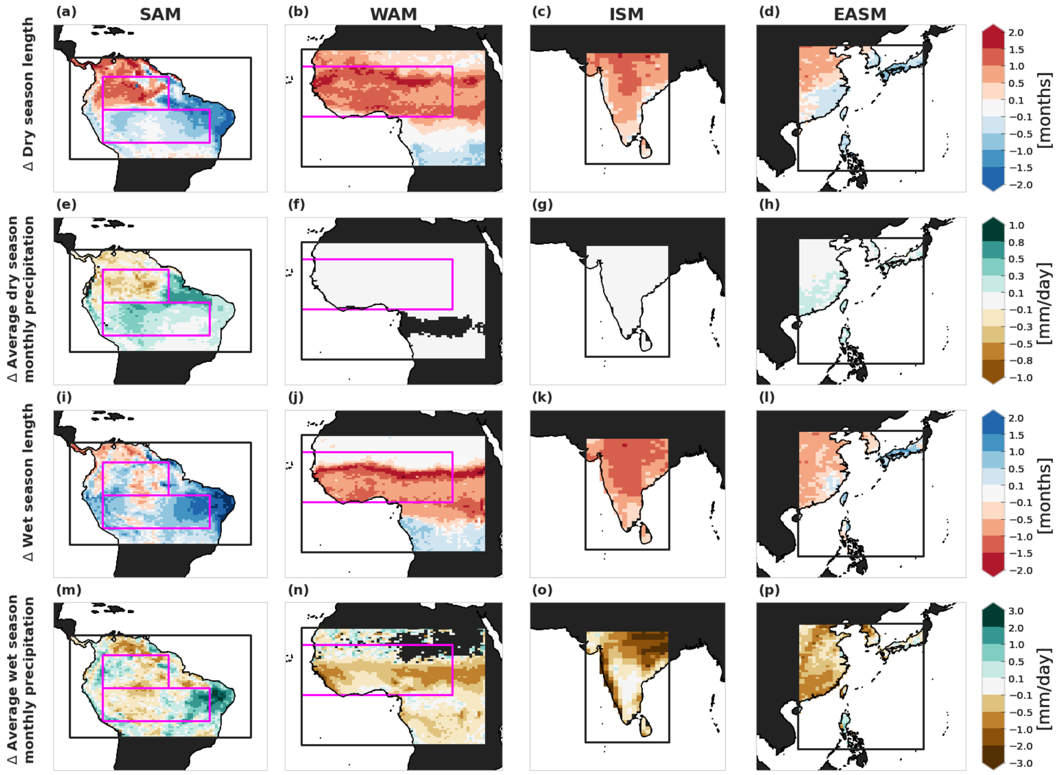

Figure 5. Changes in dry and wet season length and average monthly precipitation in HadGEM3-GC3-1MM, defined as the weak AMOC run value minus the piControl value. The four rows show the change in dry season length (a-d), average dry season monthly precipitation (e-h), wet season length (i-l) and average wet season monthly precipitation (m-p), respectively. Each column shows a different monsoon region, with the region used for defining the dry/wet season shown as a black box. See methods for further details. The magenta boxes show the regions used in Figure 4 if they are different from the black boxes. Note the scales for the change in dry and wet season lengths are inverted to match red/blue to less/more rain respectively. Some areas within the monsoon regions are black if neither model run has a dry/wet season in that area, according to our definition (see Methods). Coordinates of the boxes use to define the dry/wet season can be found in Table S4.

In the first column of Figure 4 and in Figure 1 it can be seen that while in general the sign of change is the same for the average as within the region, there is some spatial variation in the magnitude of the rainfall change. This spatial variation can be investigated through the change in the characteristics of the dry and wet seasons in the four regions. We define the dry (wet) season as the months with rainfall below (above) the 40th (60th) percentile of the whole region (see Methods for full details). Changes in dry- and wet-season rainfall and length caused by an AMOC collapse are shown only for HadGEM for the sake of clarity, as it has the most realistic Atlantic ITCZ (see Figure

S3) and highest spatial resolution (Figure 5). Note that the changes in precipitation in HadGEM are highly correlated with the changes in the other models in the monsoon regions (see Methods and Fig S6 and S7). The results agree with our previous findings: a general drying of the WAM, ISM and EASM through a longer dry season and a shorter wet season, and a more complex pattern for the SAM. In particular,

(i) the northern Amazon has a similar or longer dry season and a shorter wet season in most regions. The average dry season month also shows a reduction in precipitation. The wet season months are wetter in the western part, and drier in the eastern part, matching the pattern seen in the yearly mean (Figure 1). Yet, the rainfall reduction over the eastern part of the northern Amazon is only shown by HadGEM (Figure S7);

(ii) the southern Amazon shows a shorter and wetter dry season, but has a mixed pattern for the wet season. The western part of the southern Amazon generally has a drier and shorter wet season. The overall increase in wet season rainfall is related to the longer and much wetter wet season of the eastern edge of the southern Amazon. All piControl runs show a strong wet bias compared to observations in this southeastern Amazon region (Figure S1), so the change in rainfall might not be accurate;

(iii) in Africa, the WAM region is where the largest changes occur, with a longer dry season and a shorter wet season, especially at the southern edge of the Sahel. There is negligible change in the dry season monthly precipitation (which was already close to zero), but there is a reduction in the wet season precipitation. The only outlier is the Congo region, which benefits from a a shorter dry season and a longer (but drier) wet season due to the southward shift of the Atlantic ITCZ;

(iv) for the ISM, the drying is more predominant in the wet season. While the dry season is longer by up to one month inland, the wet season is shorter by at least a month almost everywhere and has significantly drier months in the north-east;

(v) the EASM has a mixed change in the dry season: the northern part has a longer and the southern a shorter dry season, with little change in the average precipitation. The overall drying is more drastic in the wet season, similarly to the ISM, with an overall shorter wet season and drier months.

3 Discussion and Conclusions

The four monsoon systems investigated in this work are vital parts of the global climate. Nearly three-quarters of the world's population is affected by monsoons, making them a high priority regarding possible impacts of anthropogenic global warming. This work is the first one to compare the effect of an AMOC collapse on monsoon systems in multiple CMIP6 GCM experiments which apply the same hosing scenario.

While the four models used in this study have different Atlantic ITCZ biases (Figure S3), their agreement on the pattern of the precipitation response to an AMOC collapse (Figures 2, S5 and S6 and Tables S2 and S3) is a strong case for the robustness of that pattern (Figures 1 and 3).

The overall response structures are remarkably consistent across models, both geographically and seasonally (Figure S5). The WAM, ISM and EASM show an overall drying with a shorter wet season and longer dry season in response to an AMOC collapse. The SAM shows a more spatially dependant pattern, with an overall annual increase in rainfall, a higher increase of annual precipitation and shorter dry season in the south and less pronounced change in the north.

The year-long reduction in precipitation associated with WAM, ISM and EASM would likely have severe ecological and socio-economic impacts. The effect of an AMOC collapse on the SAM and, hence, on the Amazon rainforest, is more uncertain. (Parsons et al., 2014) showed that even with an overall decrease in yearly rainfall sums over the region, a shorter dry season leads to increased productivity in the Amazon rainforest. However, the effect on the SAM dry season shown in this work is complex: in the northern Amazon, there is a shift of the seasonal cycle to later in the year in all models, and also an increase in dry season length. To understand the effect this would have on the rainforest requires additional modelling considering the vegetation response. On the other hand, the effect on the southern Amazon is different: more overall rainfall and a shortened and wetter dry season. This southern Amazon region is also the one shown to be losing resilience faster in the past decades (Boulton et al., 2022) and therefore may be more susceptible to changes in rainfall. This relative complexity in Amazon rainfall response may be the reason for the contrasting results of past models (Stouffer et al., 2006; Jackson et al., 2015) with regards to the effect of an AMOC collapse on the Amazon. The agreement of four different GCM experiments allows us to conclude that the overall effect of an AMOC collapse on the Amazon could counteract precipitation reductions projected for future global warming scenarios (see Arias et al. (2021)).

This work presents the effects of an AMOC collapse in tropical monsoon systems, inferred from simulations of the NAHosMIP project. Detailed analyses of many of the relevant physical processes at play in the models have already been presented in works on earlier hosing experiments, and have been identified in our results (Orihuela-Pinto et al., 2022; Good et al., 2021; Chang et al., 2008; Yu et al., 2009).

There is considerable uncertainty in the impact future global warming will have on monsoon rainfall (Arias et al., 2021; Wang et al., 2021; Moon & Ha, 2020). We show that our models agree much more for AMOC hosing experiments than they do for other CMIP6 warming experiments. Our work thus allows us to constrain projections in this high-uncertainty region.

The key property of the impacts discussed in this work is that they are practically irreversible. Whilst the direct impacts on monsoon rainfall from anthropogenic forcing could be reversed if the temperature is returned to pre-industrial levels, the collapse of the AMOC is permanent in the experiments considered in this study, something that was not certain in many previous hosing experiments. The impacts presented in this work could thus represent practically irreversible long-term changes that would persist even after a return to pre-industrial conditions.

Regardless of whether or not it is combined with increased temperatures, an AMOC collapse would result in a major rearranging of the global monsoon systems. This work shows that this rearrangement will have unfavorable effects on the WAM, ISM and EASM and a more uncertain effect on the SAM and the Amazon rainforest.

Methods

Model runs and processing of the outputs

We use the uniform hosing experiments from the North Atlantic Hosing Model Intercomparison study (NAHosMIP, Jackson et al. (2022)). These experiments start from the respective pre-industrial control (piControl) runs of CMIP6 models, and apply a 0.3Sv uniform hosing from 50°N to the Bering Strait. This hosing is applied for a given length of time and then stopped, after which the model continues to run. In the models we consider, the AMOC remains in the weak state after the hosing is turned off. For HadGEM, CanESM and CESM, we use the u03-r50 experiments, in which the hosing has been halted after 50 years. For IPSL, we use the u03-r100 experiments, in which the hosing has been halted after 100 years.

For consistent comparison we use 80 years from each of the different model runs. As the AMOC takes a few years to settle into a stable state after the hosing is turned off, we take the last 80 years from HadGEM and CanESM, years 100-180 from CESM and years 60-140 from IPSL. For all models we use the first 80 years from the piControl.

For the comparison with the observational GPCP dataset the model outputs are regridded to a regular 2.5° grid. For calculation of the ensemble mean the model outputs are regridded to the coarsest-resolution model grid, that of the CanESM5 model. When correlating the HadGEM3-GM3-1MM output with the other three models, the HadGEM outputs are regridded to the respective model grid. All regridding is done using a first order conservative remapping.

4xCO2 experiments are taken from the CMIP6 abrupt-4xCO2 experiments, where an instantaneous quadrupling of the pre-industrial atmospheric CO_2 concentration is imposed and this concentration is kept constant. As the AMOC takes a few years to react to this we take years 60-140 from all models, using 80 years for consistent comparison with the NAHosMIP runs. We also use the CMIP6 historical runs, in which the anthropogenic forcings of 1850-2014 are applied to the climate, starting from some point in the piControl run. For all models, the r1i1p1f1 ensemble member is used, with the exception of HadGEM3, for which r1i1p1f3 is used. This is also the case for the piControl and 4xCO2 runs.

For the scenario-mip CMIP6 runs ssp585 and ssp126 we use years 2080-2100 for consistency across models. The same ensemble members are used as above, except for CESM2 where we use r4i1p1f1 in ssp126 and r10i1p1f1 in ssp585.

Observational Datasets

For comparison with model results and calculation of the ITCZ latitude (which requires precipitation data over land and sea), we use the GPCP Precipitation data provided by NOAA/OAR/ESRL PSL, Boulder, Colorado, USA (Adler et al., 2018) available for 1979-2020. For all other precipitation analyses we use the GPCC Full Data Monthly Product Version 2020 at 0.25° from 1921 to 2019 (the first 20 years are not used due to the paucity of measurements in the regions of interest) (Schneider et al., 2020).

For the observed AMOC strength (Figure S4) the RAPID AMOC monitoring project data is used (Frajka-Williams et al., 2021).

ITCZ calculation

The ITCZ latitude is calculated following Good et al. (2021) to evaluate the model performance and effect of AMOC collapse.

The Atlantic ITCZ latitude is calculated in the area 35–15°W 15°S–15°N as a precipitation-weighted mean, as follows:

$$\phi_{itcz} = \sum_i \frac{\mathrm{P}_{35-15^\circ W,\phi_i} \cdot \phi_i}{\mathrm{P}_{35-15^\circ W,15^\circ S-15^\circ N}} \tag{1}$$

Where $\mathrm{P}_{35-15^\circ W,\phi_i}$ is the zonally averaged precipitation at latitude ϕ_i, and $\mathrm{P}_{35-15^\circ W,15^\circ S-15^\circ N}$ is the precipitation averaged over the whole region. Each latitude is thus weighted by the precipitation at that latitude.

The same procedure is repeated in the Indian and Pacific oceans for the following areas: 55°E-95°E, 15°S-15°N and 120°E-95°W,15°S-15°N, respectively.

The ITCZ and AMOC strength in the different models

When compared to the observed seasonal cycle of the Atlantic ITCZ (hereafter simply ITCZ) the models can be divided into two groups (Figure S3 (a)-(d)): (i) The CanESM and IPSL piControl runs have ITCZ latitudes going much further south (around 8°) in the December – March season (DJFM) than in observations. Their ITCZ varies more than 13° in latitude in a year, whilst the change in the average ITCZ seasonal cycle in the observation is 8.5 °. It turns out that these two models only have a small ($\leq 1°$) latitudinal shift in the ITCZ between the control and weak AMOC; (ii) HadGEM and CESM have a more realistic seasonal cycle of the ITCZ latitude, where the southward bias of the piControl is about 1 ° for all months. Compared to the Atlantic Ocean, the biases in simulated ITCZ latitudes in the piControl run relative to the observations are smaller in the Indian and Pacific Oceans (see Fig S8).

On the other hand, those models which have a more realistic latitudinal shift are also those which have a stronger piControl AMOC at 26.5N: In CanESM and IPSL the piControl AMOC has a strength of 11.27 Sv and 12.49 Sv respectively, and a post-hosing weak AMOC of 6.53 Sv and 5.20 Sv (Figure S4). HadGEM and CESM, on the other hand, have a much stronger piControl AMOC at 16.46 Sv and 17.39, respectively, and a post-hosing AMOC at 5.82 Sv and 8.70 Sv. The RAPID array obsevational measurements of the AMOC strength at 26.5N have a mean of 16.9 ± 4.6 Sv in 2004-2020 (Frajka-Williams et al., 2021), closer to HadGEM and CESM than to the other two models. Note, however, that these are historical observations and thus include the effect of anthropogenic forcings, and cannot be directly compared with the piControl simulations.

However although the collapsed AMOC has a similar strength in all four models, there are still major differences between the post-collapsed ITCZ cycles of the two groups of models. It is more likely that other properties of the IPSL and CanESM models cause both an extended ITCZ excursion to the south and a weaker piControl AMOC. In the CMIP6 Atmospheric Model Intercomparison Project (AMIP) experiments CanESM and IPSL have a seasonal ITCZ cycle much closer to the observations, without the southward excursion (Fig S9). As the AMIP models are forced with historical SSTs, the biases in the piControl runs of CanESM and IPSL are likely due to either biases in the modelled SST fields or in the SST-precipitation interactions in these models. Note, however, that the AMIP models include historical forcings which are absent in the piControl runs. Thus, for a reliable estimate of the magnitude (and not only the sign) of the precipitation change due to an AMOC collapse, further work should focus on the differences in the AMOC and SST biases of the different models.

Defining dry and wet seasons

The dry and wet seasons are defined using a non-parametric approach for consistency across monsoon regions. First, percentile boundaries are calculated for each region using all gridpoints and years. The dry or wet season months in a given year and gridpoint are then all the months that have less or more rain than the chosen percentile boundary of the region. The 40th and 60th percentile are chosen for the dry and wet season, respectively. The dry season percentile is chosen such that for the SAM the dry season monthly rainfall limit is about 100 mm, which is the mean monthly evapotranspiration value of tropical forests (below this value evapotranspiration exceeds rainfall, see (Carvalho et al., 2021)).

The averaged dry (wet) season length is then the mean of dry (wet) season length over all years. The total dry (wet) season precipitation is, accordingly, the sum of rainfall in all months of the season, which is again averaged over all years to give the average total dry (wet) season precipitation. However, when comparing seasonal rainfall across runs with different season lengths, the total precipitation will be biased by the difference in season length. An average dry (wet) season monthly precipitation value is therefore defined by dividing the total dry (wet) season rainfall in a year by the length of the dry (wet) season in that year, and the average is calculated as

$$p_{i,\mathrm{dry,avg}} = \frac{1}{T}\sum_{t=1}^{T} \frac{p_{i,t,\mathrm{dry}}}{x_{i,t,\mathrm{dry}}}\,, \tag{2}$$

where $p_{i,t,\mathrm{dry}}$ and $x_{i,t,\mathrm{dry}}$ are respectively the total dry season precipitation and dry season length in grid-point i in year t, and the sum is over all years T.

When comparing these values between the piControl and weak AMOC model runs, there are two ways to define the dry (wet) season for the weak AMOC run. The first is to use the regions' percentile boundary values calculated for the piControl run, and apply them as the limit defining the weak AMOC seasons. The second is to independently calculate new percentiles for the weak AMOC precipitation and use those as the defining limits. The first option reflects the experience of an abrupt change in the AMOC, as it shows how the "known" seasons would change after a collapse. The second is more applicable to an analysis of a long-term state, as it shows what the dry (wet) season would look like in a world with a weak AMOC. As we are interested in the effect of an abrupt collapse on ecosystems and societies which are in general adapted to a given pattern and strength of seasonal rainfall, the value of interest will be the first one, which reflects how the known seasons would change.

Model bias

Figure S1 shows the difference between the piControl run for the four models and the global GPCP observations. The pattern in the yearly average precipitation bias is as follows: (i) For the SAM all models except HadGEM show an ∼2mm/day dry bias, whilst HadGEM shows a weak wet bias in the southern Amazon and a weak dry bias in the northern Amazon; (ii) For the WAM there is a small dry bias in all four models; (iii) For the ISM HadGEM and CanESM have a dry bias everywhere, whilst CESM and IPSL have a dry bias in the north and a wet bias in the south; (iv) For the EASM all models except IPSL have a wet bias, whilst IPSL has a small dry bias. The piControl run is the starting point with which we compare the collapsed AMOC state, so although the observations are historical and thus include anthropogenic forcings not present in the piControl runs, these comparisons are still informative.

Agreement between HadGEM3-GC3-1MM and other models

In Figure 5 the changes in dry and wet seasons are shown only for HadGEM. This model was chosen due to its realistic Atlantic ITCZ and its higher spatial resolution. To justify the use of HadGEM as representative of all models, Figure S7 shows the regions in which all three other models or two of the other three models show the same sign of precipitation anomaly as HadGEM, and Table S5 shows the correlation of the other models with HadGEM. These figures show the remarkable agreement between the models. The only region in the monsoon areas of interest where HadGEM does not agree with the other models is in the northeastern Amazon, where HadGEM shows a slight overall drying. However, it can be seen that the detailed seasonal response of precipitation in that region is the same in all four models (Figure 4). The annual mean in this region is the combined effect of a drying in January to June and increased rainfall in the rest of the year. It is likely that the dry region in HadGEM has a different ratio between these two effects than in the other models, but in practice has a similar response.

4 Open Research

The NAHosMIP model data is available at https://doi.org/10.5281/zenodo.7324394. The pre-industrial control, 4xCO2 and AMIP experimental data is available via the Earth System Grid Federation (ESGF) servers with information on obtaining data available from https://pcmdi.llnl.gov/CMIP6/Guide/dataUsers.html. The GPCP and GPCC precipitation datasets are available at https://psl.noaa.gov/. The RAPID observational data is available at https://rapid.ac.uk/. All code used to analyse the data and generate figures will be uploaded at https://github.com/mayaby.

Acknowledgments

MBY and NB acknowledge funding by the European Union's Horizon 2020 research and innovation programme under the Marie Sklodowska-Curie grant agreement No.956170. NB acknowledges funding by the Volkswagen foundation. NB and LCJ acknowledge funding by the TiPES project. This is TiPES contribution #X; the TiPES ('Tipping Points in the Earth System') project has received funding from the European Union's Horizon 2020 research and innovation programme under grant agreement No. 820970. NB acknowledges further funding by the German Federal Ministry of Education and Research under grant No. 01LS2001A. OS thanks the CCCma team for support. LCJ was supported by the Met Office Hadley Centre Climate Programme funded by BEIS and Defra (grant GA01101).

References

Adler, R. F., Sapiano, M. R. P., Huffman, G. J., Wang, J.-J., Gu, G., Bolvin, D., ... Shin, D.-B. (2018). The global precipitation climatology project (gpcp) monthly analysis (new version 2.3) and a review of 2017 global precipitation. *Atmosphere*, *9*(4). Retrieved from `https://www.mdpi.com/2073-4433/9/4/138` doi: 10.3390/atmos9040138

Arias, P. A., Bellouin, N., Coppola, E., Jones, R. G., Krinner, G., Marotzke, J., ... Zickfeld, K. (2021). Technical summary [Book Section]. In V. Masson-Delmotte et al. (Eds.), *Climate change 2021: The physical science basis. contribution of working group i to the sixth assessment report of the intergovernmental panel on climate change* (chap. 1). Cambridge, United Kingdom and New York, NY, USA: Cambridge University Press. Retrieved from `https://www.ipcc.ch/report/ar6/wg1/downloads/report/IPCC_AR6_WGI_TS.pdf`

Boers, N. (2021). Observation-based early-warning signals for a collapse of the Atlantic Meridional Overturning Circulation. *Nature Climate Change*, *11*(8), 680–688. Retrieved from `http://dx.doi.org/10.1038/s41558-021-01097-4` doi: 10.1038/s41558-021-01097-4

Boulton, C. A., Lenton, T. M., & Boers, N. (2022). Pronounced loss of Amazon rainforest resilience since the early 2000s. *Nature Climate Change*, *12*(March). doi: 10.1038/s41558-022-01287-8

Caesar, L., McCarthy, G. D., Thornalley, D. J., Cahill, N., & Rahmstorf, S. (2021). Current Atlantic Meridional Overturning Circulation weakest in last millennium. *Nature Geoscience*, *14*(3), 118–120. Retrieved from `http://dx.doi.org/10.1038/s41561-021-00699-z` doi: 10.1038/s41561-021-00699-z

Carvalho, N. S., Anderson, L. O., Nunes, C. A., Pessôa, A. C., Silva Junior, C. H., Reis, J. B., ... Aragão, L. E. (2021). Spatio-Temporal variation in dry season determines the Amazonian fire calendar. *Environmental Research Letters*, *16*(12). doi: 10.1088/1748-9326/ac3aa3

Chang, P., Zhang, R., Hazeleger, W., Wen, C., Wan, X., Ji, L., ... Seidel, H. (2008). Oceanic link between abrupt changes in the north Atlantic ocean and the African monsoon. *Nature Geoscience*, *1*(7), 444–448. doi: 10.1038/ngeo218

Drijfhout, S. S., Weber, S. L., & van der Swaluw, E. (2011). The stability of the MOC as diagnosed from model projections for pre-industrial, present and future climates. *Climate Dynamics*, *37*(7-8), 1575–1586. doi: 10.1007/s00382-010-0930-z

Frajka-Williams, E., Moat, B., Smeed, D., Rayner, D., Johns, W., Baringer, M., ...

Collins, J. (2021). *Atlantic meridional overturning circulation observed by the rapid-mocha-wbts (rapid-meridional overturning circulation and heatflux array-western boundary time series) array at 26n from 2004 to 2020 (v2020.1).* doi: 10.5285/cc1e34b3-3385-662b-e053-6c86abc03444

Good, P., Boers, N., Boulton, C. A., Lowe, J. A., & Richter, I. (2021). How might a collapse in the Atlantic Meridional Overturning Circulation affect rainfall over tropical South America? *Climate Resilience and Sustainability*(November), 1–13. doi: 10.1002/cli2.26

Häggi, C., Chiessi, C. M., Merkel, U., Mulitza, S., Prange, M., Schulz, M., & Schefuß, E. (2017). Response of the Amazon rainforest to late Pleistocene climate variability. *Earth and Planetary Science Letters*, *479*, 50–59. Retrieved from http://dx.doi.org/10.1016/j.epsl.2017.09.013 doi: 10.1016/j.epsl.2017.09.013

Henry, L. G., McManus, J. F., Curry, W. B., Roberts, N. L., Piotrowski, A. M., & Keigwin, L. D. (2016). North Atlantic ocean circulation and abrupt climate change during the last glaciation. *Science*, *353*(6298), 470–474. doi: 10.1126/science.aaf5529

Jackson, L. C., Asenjo, E. A. D., Bellomo, K., Danabasoglu, G., Haak, H., Hu, A., ... Swingedouw, D. (2022). Understanding AMOC stability : the North Atlantic Hosing Model Intercomparison Project. *Geoscientific Model Development Discussions*(November), 1–32. Retrieved from https://gmd.copernicus.org/preprints/gmd-2022-277/ doi: 10.5194/gmd-2022-277

Jackson, L. C., Kahana, R., Graham, T., Ringer, M. A., Woollings, T., Mecking, J. V., & Wood, R. A. (2015). Global and European climate impacts of a slowdown of the AMOC in a high resolution GCM. *Climate Dynamics*, *45*(11-12), 3299–3316. Retrieved from http://dx.doi.org/10.1007/s00382-015-2540-2 doi: 10.1007/s00382-015-2540-2

Jackson, L. C., & Wood, R. A. (2018). Hysteresis and Resilience of the AMOC in an Eddy-Permitting GCM. *Geophysical Research Letters*, *45*(16), 8547–8556. doi: 10.1029/2018GL078104

Lee, J. Y., Marotzke, J., Bala, G., Cao, L., Corti, S., Dunne, J. P., ... Zhou, T. (2021). Future global climate: Scenario-based projections and near-term information [Book Section]. In V. Masson-Delmotte et al. (Eds.), *Climate change 2021: The physical science basis. contribution of working group i to the sixth assessment report of the intergovernmental panel on climate change* (chap. 4). Cambridge, United Kingdom and New York, NY, USA: Cambridge University Press. Retrieved from https://www.ipcc.ch/report/ar6/wg1/downloads/report/IPCC_AR6_WGI_Chapter_04.pdf

Liu, W., Xie, S. P., Liu, Z., & Zhu, J. (2017). Overlooked possibility of a collapsed atlantic meridional overturning circulation in warming climate. *Science Advances*, *3*(1), 1–8. doi: 10.1126/sciadv.1601666

Liu, Y., Chiang, J. C., Chou, C., & Patricola, C. M. (2014). Atmospheric teleconnection mechanisms of extratropical North Atlantic SST influence on Sahel rainfall. *Climate Dynamics*, *43*(9-10), 2797–2811. doi: 10.1007/s00382-014-2094-8

Marzin, C., Kallel, N., Kageyama, M., Duplessy, J. C., & Braconnot, P. (2013). Glacial fluctuations of the Indian monsoon and their relationship with North Atlantic climate: New data and modelling experiments. *Climate of the Past*, *9*(5), 2135–2151. doi: 10.5194/cp-9-2135-2013

Moon, S., & Ha, K. J. (2020). Future changes in monsoon duration and precipitation using CMIP6. *npj Climate and Atmospheric Science*, *3*(1), 1–7. Retrieved from http://dx.doi.org/10.1038/s41612-020-00151-w doi: 10.1038/s41612-020-00151-w

Mosblech, N. A., Bush, M. B., Gosling, W. D., Hodell, D., Thomas, L., Van Calsteren, P., ... Van Woesik, R. (2012). North Atlantic forcing of Amazonian precipitation during the last ice age. *Nature Geoscience*, *5*(11), 817–820. doi: 10.1038/ngeo1588

Orihuela-Pinto, B., England, M. H., & Taschetto, A. S. (2022). Interbasin and interhemispheric impacts of a collapsed Atlantic Overturning Circulation. *Nature Climate Change*. doi: 10.1038/s41558-022-01380-y

Parsons, L. A., Yin, J., Overpeck, J. T., Stouffer, R. J., & Malyshev, S. (2014). Influence of the atlantic meridional overturning circulation on the monsoon rainfall and carbon balance of the American tropics. *Geophysical Research Letters*, *41*(1), 146–151. doi: 10.1002/2013GL058454

Rahmstorf, S. (2002). NAT(419,207)-circulation. , *419*(September), 207–214.

Rahmstrof, S., Crucifix, M., Ganopolski, A., Goosse, H., Kamenkovich, I., Knutti, R., ... Weaver, A. J. (2005). Thermohaline circulation hysteresis: A model intercomparison. *Geophysical Research Letters*, *32*(23), 1–5. doi: 10.1029/2005GL023655

Romanou, A., Rind, D., Jonas, J., Miller, R., Kelley, M., Russell, G., ... Schmidt, G. A. (2023). Stochastic Bifurcation of the North Atlantic Circulation Under A Mid-Range Future Climate Scenario With The NASA-GISS ModelE. *Journal of Climate*, 1 - 49. Retrieved from `https://journals.ametsoc.org/view/journals/clim/aop/JCLI-D-22-0536.1/JCLI-D-22-0536.1.xml` doi: 10.1175/JCLI-D-22-0536

Sandeep, N., Swapna, P., Krishnan, R., Farneti, R., Prajeesh, A. G., Ayantika, D. C., & Manmeet, S. (2020). South Asian monsoon response to weakening of Atlantic meridional overturning circulation in a warming climate. *Climate Dynamics*, *54*(7-8), 3507–3524. Retrieved from `https://doi.org/10.1007/s00382-020-05180-y` doi: 10.1007/s00382-020-05180-y

Schneider, U., Becker, A., Finger, P., Rustemeier, E., & Ziese, M. (2020). *Gpcc full data monthly product version 2020 at 0.25°: Monthly land-surface precipitation from rain-gauges built on gts-based and historical data.* doi: 10.5676/DWD_GPCC/FD_M_V2020_025

Stommel, H. (1961). Thermohaline Convection with Two Stable Regimes of Flow. *Tellus*, *13*(2), 224–230. doi: 10.3402/tellusa.v13i2.9491

Stouffer, R. J., Yin, J., Gregory, J. M., Dixon, K. W., Spelman, M. J., Hurlin, W., ... Weber, S. L. (2006). Investigating the causes of the response of the thermohaline circulation to past and future climate changes. *Journal of Climate*, *19*(8), 1365 - 1387. Retrieved from `https://journals.ametsoc.org/view/journals/clim/19/8/jcli3689.1.xml` doi: https://doi.org/10.1175/JCLI3689.1

Sun, Y., Clemens, S. C., Morrill, C., Lin, X., Wang, X., & An, Z. (2012). Influence of Atlantic meridional overturning circulation on the East Asian winter monsoon. *Nature Geoscience*, *5*(1), 46–49. doi: 10.1038/ngeo1326

Wang, B., Biasutti, M., Byrne, M. P., Castro, C., Chang, C. P., Cook, K., ... Zhou, T. (2021). Monsoons climate change assessment. *Bulletin of the American Meteorological Society*, *102*(1), E1-E19. doi: 10.1175/BAMS-D-19-0335.1

Wassenburg, J. A., Vonhof, H. B., Cheng, H., Martínez-García, A., Ebner, P. R., Li, X., ... Haug, G. H. (2021). Penultimate deglaciation Asian monsoon response to North Atlantic circulation collapse. *Nature Geoscience*, *14*(12), 937–941. doi: 10.1038/s41561-021-00851-9

WRCP, W. C. R. P. (n.d.). *The global monsoon systems.* Retrieved from `https://www.wcrp-climate.org/documents/monsoon_factsheet.pdf`

Yu, L., Gao, Y. Q., Wang, H. J., Guo, D., & Li, S. L. (2009). The responses of East Asian Summer monsoon to the North Atlantic Meridional Overturning Circulation in an enhanced freshwater input simulation. *Chinese Science Bulletin*, *54*(24), 4724–4732. doi: 10.1007/s11434-009-0720-3

Robust and irreversible impacts of an AMOC collapse on tropical monsoon systems: a multi-model comparison

M. Ben-Yami[1,2], P. Good[3], L. C. Jackson [3], M. Crucifix [4], A. Hu [5], O. Saenko [6], D. Swingedouw [7] and N. Boers [1,2,8]

[1]Earth System Modelling, School of Engineering and Design, Technical University of Munich, Munich, Germany
[2]Potsdam Institute for Climate Impact Research, Potsdam, Germany
[3]Met Office, Exeter, UK
[4]Earth and Life Institute, UCLouvain, Place Louis Pasteur 3, Louvain-La-Neuve, 1348, Belgium
[5]Climate and Global Dynamics Lab, National Center for Atmospheric Research, Boulder, CO 80307, USA
[6]SEOS, University of Victoria, BC, Canada
[7]Environnements et Paléoenvironnements Océaniques et Continentaux (EPOC)— Université de Bordeaux, Pessac, France
[8]Department of Mathematics and Global Systems Institute , University of Exeter, Exeter, UK

Key Points:

- A collapse of the AMOC would cause a major rearrangement of all tropical monsoon systems
- Four state-of-the-art climate models show remarkable agreement on the effects of an AMOC collapse
- These impacts are practically irreversible

Corresponding author: M. Ben-Yami, `maya.ben-yami@tum.de`

Abstract

A collapse of the Atlantic Meridional Overturning Circulation (AMOC) would have substantial impacts on global precipitation patterns, especially in the vulnerable tropical monsoon regions. We assess these impacts using four state-of-the-art climate models with bistable AMOC. Spatial and seasonal patterns of precipitation change are remarkably consistent across models. We focus on the South American Monsoon (SAM), the West African Monsoon (WAM), the Indian Summer Monsoon (ISM) and the East Asian Summer Monsoon (EASM). Models consistently suggest substantial disruptions for WAM, ISM and EASM with shorter wet and longer dry seasons (-29.07%,-18.76% and -3.78% ensemble mean annual rainfall change, respectively). Models also agree on changes for the SAM, suggesting rainfall increases overall, in contrast to previous studies. These are more pronounced in the southern Amazon (+43.79%), accompanied by decreasing dry-season length. Consistently across models, our results suggest major rearranging of all tropical monsoon systems in response to an AMOC collapse.

Plain Language Summary

The Atlantic Meridional Overturning Circulation (AMOC) is a key element of the Earth's climate system, transporting large amounts of heat and salt northward in the upper layers of the Atlantic ocean. Although its likelihood remains highly uncertain, a collapse of the AMOC in response to anthropogenic climate change would have catastrophic ecological and societal consequences. This is especially true in the vulnerable monsoon regions of the tropics. Yet, the precise effects of an AMOC collapse on the tropical monsoon systems remain unclear. We take advantage of a climate model intercomparison project, and provide a detailed and systematic analysis of the irreversible seasonal impacts of an AMOC collapse on the major tropical monsoon systems. We find remarkable, previously unseen, agreement between four independent state-of-the-art climate models. Consistently across models, our results suggest major rearranging of all tropical monsoon systems in response to an AMOC collapse.

1 Introduction

The Atlantic Meridional Overturning Circulation (AMOC) is a key element of the Earth's climate system, transporting large amounts of heat and salt northward in the upper layers of the Atlantic ocean. Paleoclimate proxy evidence as well as theoretical considerations suggest that the AMOC is bistable, with a second, substantially weaker circulation mode in addition to the present strong mode (Henry et al., 2016; Stommel, 1961; Rahmstorf, 2002). The question whether the AMOC is bistable in comprehensive climate models has been intensely debated in recent years and a rising number of such models exhibit a bistable AMOC (Y. Liu et al., 2014; W. Liu et al., 2017; Jackson & Wood, 2018; Romanou et al., 2023). Concerns have been raised that the AMOC might collapse to its weak state in response to enhanced freshwater inflow into the North Atlantic due anthropogenic warming and resulting Greenland ice sheet melting (W. Liu et al., 2017), although the 6th assessment report (AR6) of the International Panel on Climate Change (IPCC) concludes that such a collapse has moderate likelihood to happen before 2100 (Arias et al., 2021). Studying a potential AMOC collapse is however of great interest given the severe global impacts it would have. There are several lines of proxy-based evidence suggesting that the AMOC has indeed weakened in the last decades to centuries (Caesar et al., 2021) and comprehensive models predict that it will weaken further under anthropogenic global warming (Lee et al., 2021). In addition, evidence that the recent AMOC weakening might be associated with a decrease of stability of the current circulation mode has been identified in sea-surface temperature (SST) and salinity based fingerprints of the AMOC strength (Boers, 2021).

If the AMOC were to collapse, the reduced northward heat transport would cause a relative cooling of the northern hemisphere, and the change in inter-hemispheric energy transport would lead to a shift of the thermal equator and hence a southward shift of the inter-tropical convergence zone (ITCZ) (Jackson et al., 2015). The subsequent global-scale reorganization of the atmospheric circulation would have far-reaching effects in the Pacific as well as in the Atlantic (Orihuela-Pinto et al., 2022). As the ITCZ is the main source of tropical rainfall, an AMOC collapse and associated southward ITCZ shift would likely have substantial consequences for the tropical monsoon systems. Given their socioeconomic and ecological importance, a detailed analysis of the impacts of an AMOC collapse on these monsoon systems is needed. Over half of the world's population live in climates dominated by tropical monsoons (Moon & Ha, 2020; Wang et al., 2021). Most of these are in developing countries, where land use is dominated by agriculture, so depends heavily on the rain the monsoons bring. These regions are thus vulnerable to any changes in the characteristics of the monsoon rains, whether they are changes in the timing or the amount of rainfall (WRCP, n.d.). This makes tropical monsoon regions a high priority regarding possible impacts of anthropogenic global warming (Wang et al., 2021).

There exist multiple lines of proxy evidence to assess the impacts of an AMOC collapse on the tropical monsoon systems during past climate conditions (Sun et al., 2012; Sandeep et al., 2020; Häggi et al., 2017; Mosblech et al., 2012; Wassenburg et al., 2021; Marzin et al., 2013). To study the effects in more detail and for present-day climate conditions, so-called hosing experiments in general circulation models (GCMs) are used, in which freshwater is added to a region of the north Atlantic for a long period of time, forcing the AMOC to weaken and potentially collapse to a weaker state. Some studies have also focused on individual monsoon systems such as the South American Monsoon (SAM) (Good et al., 2021; Parsons et al., 2014), the West African Monsoon (WAM) (Chang et al., 2008), the Indian Summer Monsoon (ISM) (Sandeep et al., 2020; Marzin et al., 2013) and the East Asian Summer Monsoon (EASM) (Yu et al., 2009). Most studies find an overall decrease in annual mean precipitation of the different monsoon systems. For tropical South America, however, older simulations suggesting increased annual rainfall sums (Stouffer et al., 2006) are in contrast with more recent modelling studies suggesting decreases (Jackson et al., 2015). In addition, both Parsons et al. (2014) and Good et al. (2021) note that it is important to analyse the atmospheric response throughout the seasonal cycle. Specifically, Parsons et al. (2014) find that a wetter dry season after an AMOC collapse increased the overall Amazon vegetation productivity. The overall sign of the precipitation change over tropical South America in response to an AMOC collapse remains debated. This debate is complicated by the fact that there has been no cross-model AMOC hosing comparison since (Stouffer et al., 2006), and in general it is difficult to compare the impacts in experiments with different hosing scenarios.

The bi-stability of the AMOC has long been supported by theory, simple and intermediate-complexity models (Stommel, 1961; Rahmstrof et al., 2005), as well as the paleoclimate data record (Rahmstorf, 2002; Henry et al., 2016). Nevertheless, many GCMs do not exhibit the hysteresis associated with bi-stability (Y. Liu et al., 2014; Drijfhout et al., 2011), although more recent studies do find a persistent weak state (Jackson & Wood, 2018; Romanou et al., 2023). The North Atlantic Hosing Model Intercomparison Project (NAHosMIP) compares eight different models from the sixth phase of the Climate Model Intercomparison Project (CMIP6), aiming to investigate AMOC response and associated hysteresis (Jackson et al., 2022). Four out of the eight studied models exhibit a bistable AMOC, and this allows for a unique opportunity to investigate the effects of an AMOC collapse across models. Not only do all four models use the same hosing scenario, but the bistability of their AMOC allows us to investigate the permanent and practically irreversible impacts of the stable weak AMOC state that occurs after the hosing has been stopped. This is in contrast to most AMOC hosing studies, in which the hosing is continuously applied during the study period.

The different models of NAHosMIP exhibit a range of different patterns and biases, and thus comparing the effect of an AMOC collapse across models allows us to make robust statements on its effect on tropical precipitation. In this study we use results from the four models in NAHosMIP that remain in the weak state after the hosing is stopped: HadGEM3-GC3-1MM, CanESM5, CESM2 and IPSL-CM6A-LR (hereafter abbreviated as HadGEM, CanESM, CESM and IPSL). We compare spatial precipitation fields from the the control runs of these models (piControl) to scenarios in which a constant 0.3 Sv of hosing is applied over the North Atlantic for 50 years (100 years for the IPSL model), thus weakening the AMOC. After the hosing is stopped the AMOC remains in the weak state (see Methods for more details).

2 Results

2.1 Global change in precipitation

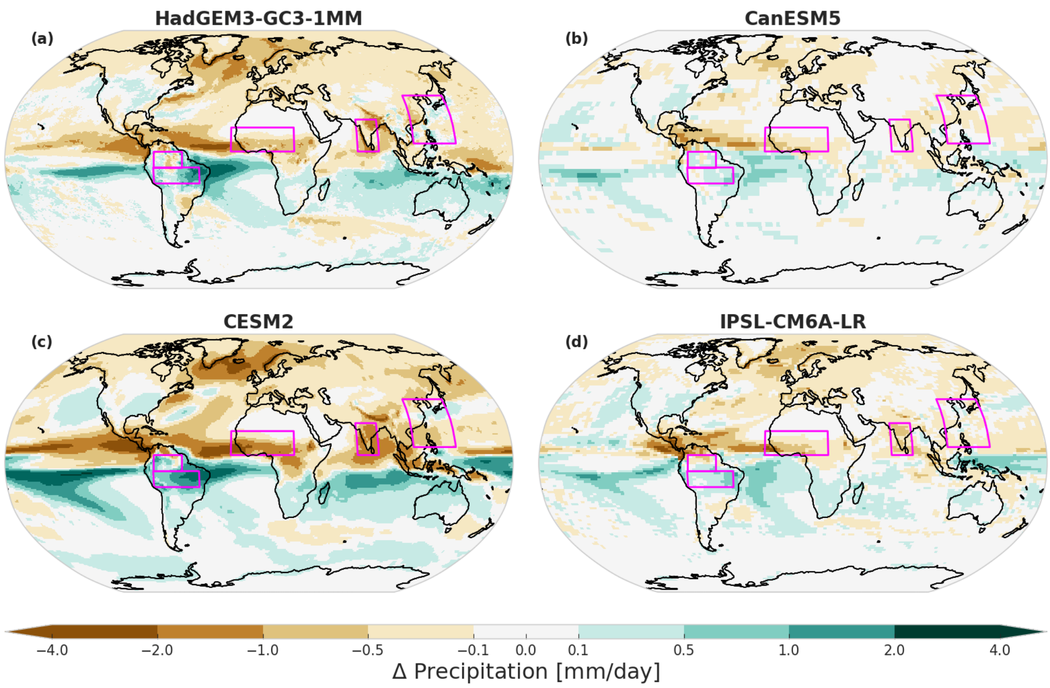

Figure 1. Modelled impacts of an AMOC collapse on global precipitation. Average precipitation shifts (weak AMOC run minus piControl run) for a. HadGEM3, b. CanESM, c. CESM, and d. IPSL. Note the southward ITCZ shift and the general pattern of Northern-Hemisphere drying and Southern-Hemisphere wettening in response to an AMOC collapse, shared by all models. The magenta boxes show the monsoon regions investigated in this work: the two parts of the SAM as well as the WAM, ISM, and EASM (see Methods and Table S1).

The model control runs have biases when compared to observations (see Figure S1). To understand the effect of an AMOC collapse on global precipitation, it is therefore more informative to analyse the differences between the post- and pre-hosing model runs than between the post-hosing runs and observations. In the following we will in general refer to the post-hosing collapsed state as the weak AMOC. The resulting pattern of global precipitation shifts in response to an AMOC collapse is then remarkably similar in all four models (Figures 1(a)-(d) and S2): (i) a southward shift of the ITCZ and overall increased (decreased) precipitation over the southern (northern) hemisphere; (ii) a general reduction of precipitation of the higher latitudes; (iii) reduced precipitation in all monsoon regions except the SAM; and (iv) increased precipitation over most of the Amazon, especially in the east.

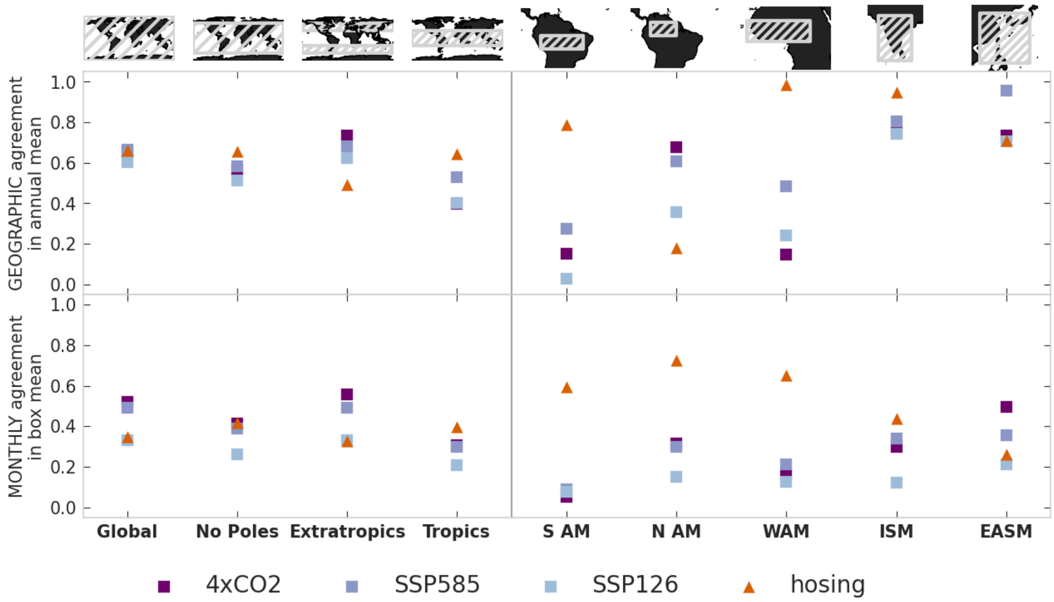

Figure 2. Model agreement in the NAHosMIP experiments compared to the agreement in CMIP6 warming experiments. (a) The fraction of gridcells in a given geographic region that agree on the sign of change in the annual mean rainfall. (b) The fraction of months in a year that agree on the sign of change in the mean monthly rainfall in the given box. The square markers show the agreement for the 4xCO2 (purple), SSP585 (lilac) and SSP126 (light blue) experiments. The triangular orange marker shows the agreement of the hosing experiments. The regions of analysis are defined in Tables S1 and S2, and are shown as grey dashed boxes on the maps in the top row. A horizontal grey line separates the values for the global boxes from the regional monsoon boxes. The exact values are given in Tables S2 and S3.

The four models show a remarkable agreement on the sign of precipitation changes in the tropics (20°S-20°N) in response to an AMOC collapse. The fraction of land in which the sign of change is consistent in the four models is 0.64 in the tropics, and is as large as 0.99 in some of the individual monsoon regions (see Table S2 and Figure 2). The agreement in the seasonal cycle change is also especially high in the Atlantic monsoon regions (Table S3). Notably, in the tropics the agreement between these four models on the impacts of an AMOC collapse are consistently higher than the agreement found in different CMIP6 warming experiments (Figure 2). As CMIP6 models are known to have inconsistent precipitation predictions in the tropics (Lee et al., 2021; Moon & Ha, 2020; Wang et al., 2021), the higher agreement found in the hosing experiments is even more remarkable.

Whilst the overall pattern of change in the four models subsequent to an AMOC collapse is in agreement, the magnitude of the precipitation change varies. CanESM and IPSL have a comparably small change in precipitation following an AMOC collapse, of the order of 0.5 mm/day in the monsoon regions (Figure 1). The model with the largest precipitation change is CESM, with a precipitation change over the SAM, ISM and WAM in CESM of the order of 2-3 mm/day, with a slightly smaller change in the EASM. HadGEM

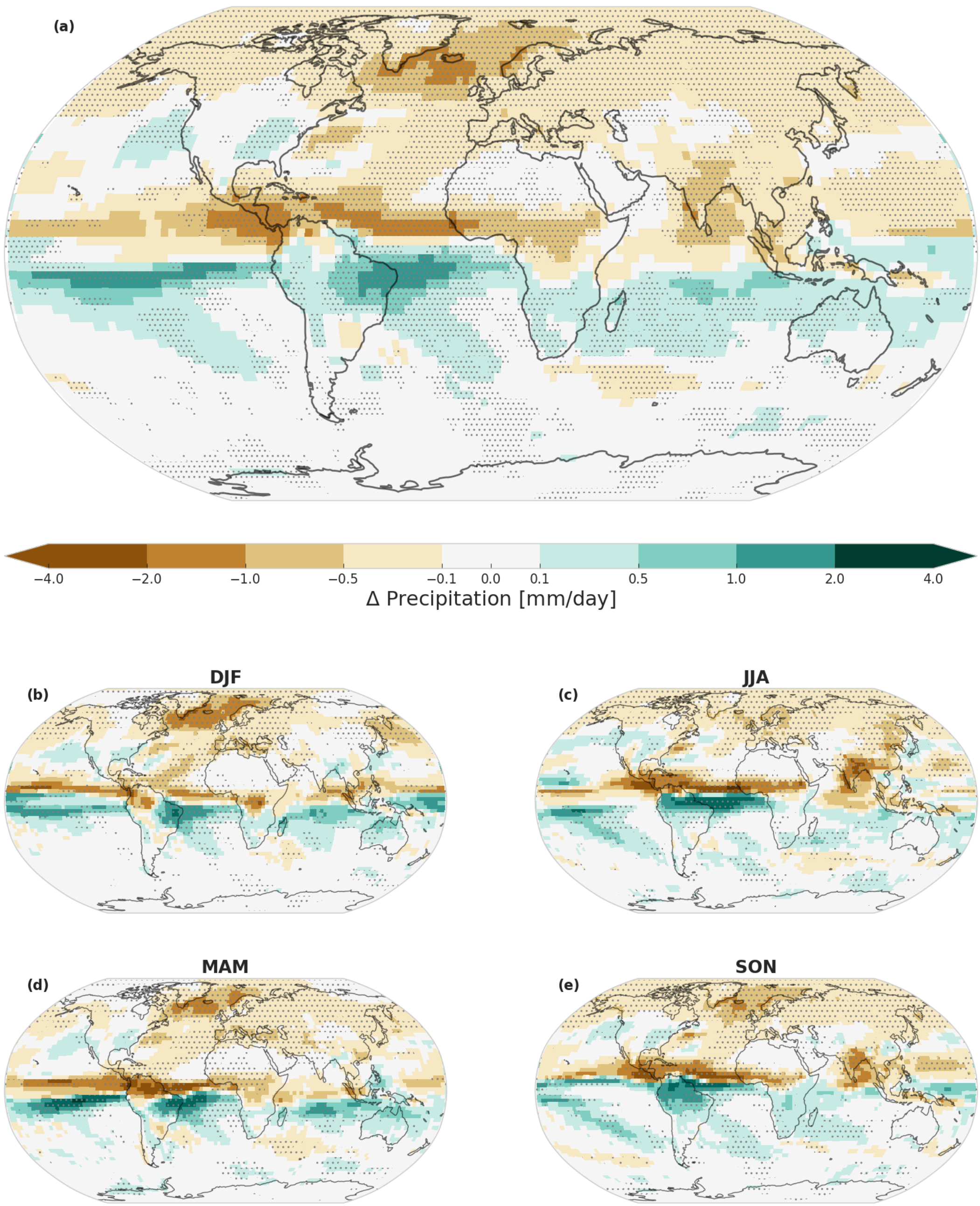

Figure 3. Average precipitation anomaly (weak AMOC run minus piControl run) for the ensemble mean of the four models. Figure (a) shows the annual mean, whilst Figures (b)-(e) show the season anomalies in DJF, JJA, MAM and SON, respectively. The stippling in each Figure indicates regions in which all four model anomalies agree in sign for that mean.

is midway between the two extremes with changes on the order of 1 mm/day. HadGEM also has a more complex precipitation change pattern for the SAM, with less rainfall over about half of the northern Amazon region and more rainfall over the rest of the region.

Even in light of the differences in magnitude, the agreement between the models is remarkable, given that previous generations of models have shown considerably stronger differences and inconsistencies (for example, Jackson et al. (2015) showed a drying over almost all of the Amazon, in contrast to the multi-model comparison in (Stouffer et al., 2006)). This similarity in our models justifies a calculation of the ensemble mean precipitation anomaly (Figure 3). The ensemble mean shows the same pattern as described above, with a drying of all monsoon regions except the SAM. The ensemble mean percentage changes in rainfall in the monsoon regions are (Figure S2): +5.2% in the Northern Amazon, +43.79% in the Southern Amazon, -29.07% in the WAM, -18.76% in the ISM and -3.78% in the EASM.

To understand the different magnitudes of model responses to an AMOC collapse we analyse the seasonal cycle of the Atlantic ITCZ following (Good et al., 2021) (see Methods). A smaller shift of the Atlantic ITCZ after an AMOC collapse should result in a smaller precipitation anomaly, and this is reflected in the respective Atlantic ITCZ shifts of the models (Figure S3 (a)-(d)). IPSL and CanESM have only a small ($\leq 1^\circ$) latitudinal shift in the Atlantic ITCZ between the control and weak AMOC, whilst the shift in HadGEM and CESM is a few times larger. The latter two also have a seasonal Atlantic ITCZ cycle which is closer to the observations (see Methods for details). The ordering of magnitudes is also mirrored in the amount the model AMOC weakens from the piControl to the weak state in the respective models (Figure S4).

2.2 Changes in the seasonal cycle

Whilst the pattern of annual mean rainfall anomaly is informative for understanding the global effect of an AMOC collapse, the effect on the major tropical monsoon systems is by definition highly seasonally dependent. We investigate the seasonal change in rainfall in two ways. First, calculating the average seasonal cycle in the whole of a given monsoon region, and second, calculating the geographic pattern of change in dry and wet seasons in these regions.

All piControl model runs match the overall pattern of the observed seasonal rainfall, but there are considerable biases in some cases (Figure 4). Their strengths depend on the region and model, with no model standing out as the best one in matching the observations across regions. For example, the best match between observations and control runs for the WAM and ISM is in CESM, but CanESM reproduces the southern Amazon rainfall better. CanESM, on the other hand, has the largest biases of any model in the northern Amazon and the ISM, with a difference of over 6 mm/day in the ISM wet season.

As discussed above, the sign of this monthly precipitation change is overall in agreement between models (Figures 2b and S5b and Table S3). In general there is high agreement in the hosing experiments for the SAM and WAM and slightly less for the ISM and EASM, which is likely due to the former being directly impacted by the southward shift of the Atlantic ITCZ.

The pattern of seasonal cycle change present in these models is: (i) The southern Amazon gains a small amount of precipitation in all months, with the exception of CanESM showing a small precipitation decrease in the January-to-March part of the wet season (Figure 4a). The overall gains are in line with a southward shift of the Atlantic ITCZ, since this box extends from 5° S down to 15° S, that is, on the edge of the Atlantic ITCZ extent. A southward shift of the Atlantic ITCZ therefore brings more of the austral summer precipitation into this area; (ii) The northern Amazon has the most complex pat-

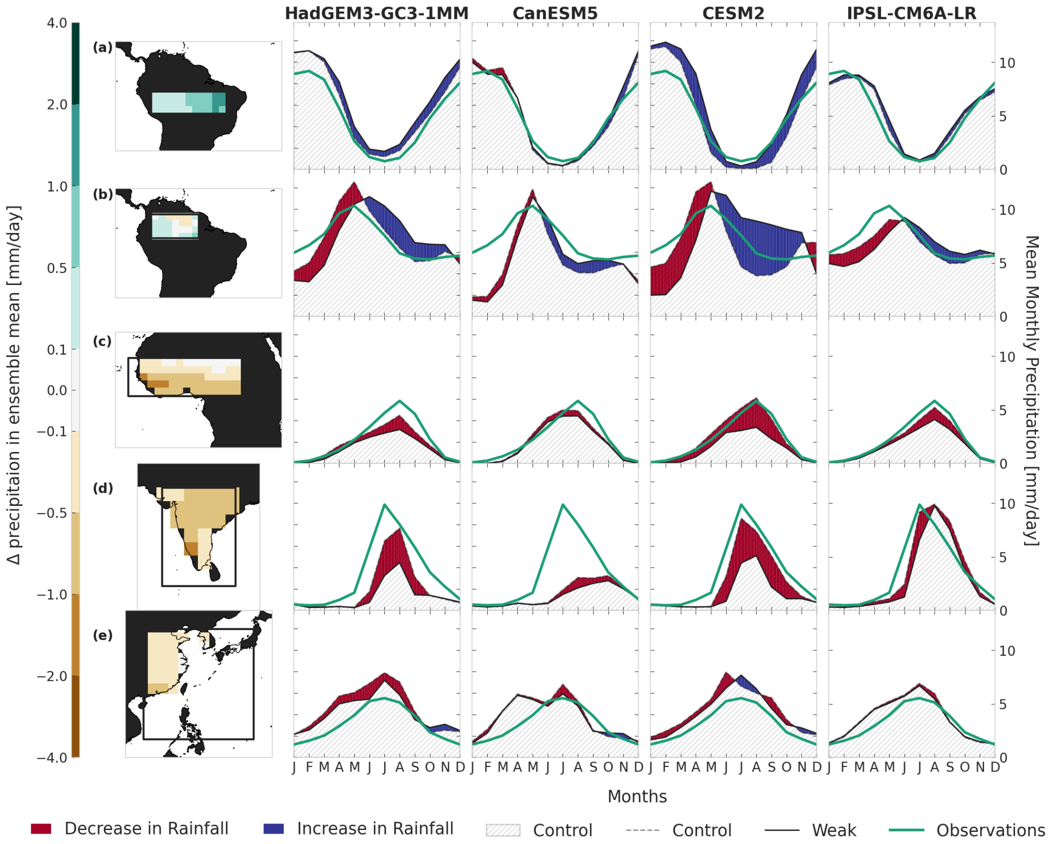

Figure 4. Changes in the seasonal cycle due to an AMOC collapse in two parts of the SAM (a,b), as well as in the WAM (c), ISM (d), and EASM (e). The first column shows the ensemble mean average yearly precipitation change in the given region (i.e., average over all four models). Taking this ensemble mean is justified by the high model agreement as identified above. The remaining columns show the change in precipitation from the average seasonal cycle in the pi-Control (dot-dashed line) to the weak AMOC run (solid line) for the four different models. The area under the graph is shaded in red where the rainfall decreases and in blue where it increases in response to an AMOC collapse. The area common to both is marked by black hatches. The observed seasonal cycle in shown as the turquoise line. Coordinates for the monsoon boxes can be found in Table S1.

tern, with reduced rainfall in the piControl wet season and increased rainfall in the pi-Control dry season (Figure 4b). This is due to a combined shift in time of the wet season to later in the year and a reduction in the overall rainfall. It should be noted that this region also has a complex spatial pattern of changing rainfall in addition to the seasonal pattern (see Figures 1, 3 and 5); (iii) The WAM has a clear pattern (Figure 4c), showing decrease in rainfall during the wet season in all models. In CESM this is a 50% rainfall decrease, and in the other models closer to 5-10%. Since the WAM is at the northern edge of the Atlantic ITCZ range, such a drying is to be expected from a southward shift of the ITCZ; (iv) The ISM has a similar pattern to the WAM, with a substantial loss of rainfall during the wet season (Figure 4d); and (v) The EASM shows a general drying which is relatively small in all models. All models also show a small increase in dry-season rainfall, but both these changes are too small to change the amplitude, timing or structure of the overall seasonal cycle. CESM also shows a shift of the peak wet season rainfall from June to August (Figure 4e).

The magnitudes of all these changes in the different models are in line with the shift in the Atlantic ITCZ - the larger the shift, the larger the precipitation change, independently of the piControl model bias.

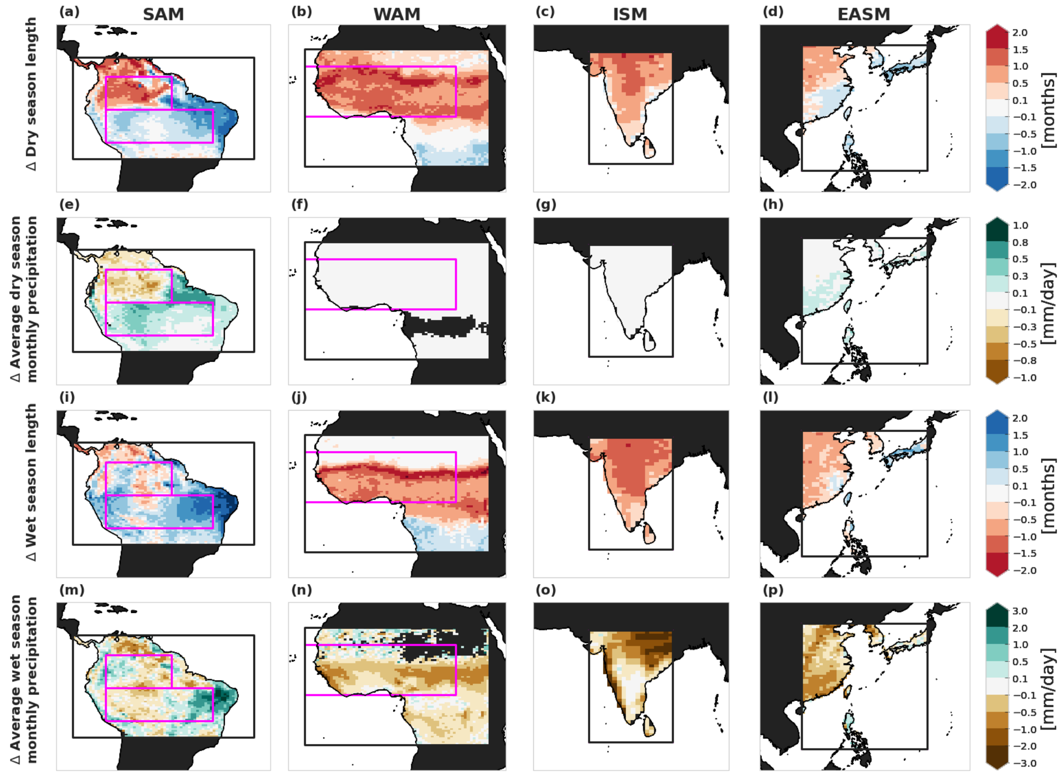

Figure 5. Changes in dry and wet season length and average monthly precipitation in HadGEM3-GC3-1MM, defined as the weak AMOC run value minus the piControl value. The four rows show the change in dry season length (a-d), average dry season monthly precipitation (e-h), wet season length (i-l) and average wet season monthly precipitation (m-p), respectively. Each column shows a different monsoon region, with the region used for defining the dry/wet season shown as a black box. See methods for further details. The magenta boxes show the regions used in Figure 4 if they are different from the black boxes. Note the scales for the change in dry and wet season lengths are inverted to match red/blue to less/more rain respectively. Some areas within the monsoon regions are black if neither model run has a dry/wet season in that area, according to our definition (see Methods). Coordinates of the boxes use to define the dry/wet season can be found in Table S4.

In the first column of Figure 4 and in Figure 1 it can be seen that while in general the sign of change is the same for the average as within the region, there is some spatial variation in the magnitude of the rainfall change. This spatial variation can be investigated through the change in the characteristics of the dry and wet seasons in the four regions. We define the dry (wet) season as the months with rainfall below (above) the 40th (60th) percentile of the whole region (see Methods for full details). Changes in dry- and wet-season rainfall and length caused by an AMOC collapse are shown only for HadGEM for the sake of clarity, as it has the most realistic Atlantic ITCZ (see Figure

S3) and highest spatial resolution (Figure 5). Note that the changes in precipitation in HadGEM are highly correlated with the changes in the other models in the monsoon regions (see Methods and Fig S6 and S7). The results agree with our previous findings: a general drying of the WAM, ISM and EASM through a longer dry season and a shorter wet season, and a more complex pattern for the SAM. In particular,

(i) the northern Amazon has a similar or longer dry season and a shorter wet season in most regions. The average dry season month also shows a reduction in precipitation. The wet season months are wetter in the western part, and drier in the eastern part, matching the pattern seen in the yearly mean (Figure 1). Yet, the rainfall reduction over the eastern part of the northern Amazon is only shown by HadGEM (Figure S7);

(ii) the southern Amazon shows a shorter and wetter dry season, but has a mixed pattern for the wet season. The western part of the southern Amazon generally has a drier and shorter wet season. The overall increase in wet season rainfall is related to the longer and much wetter wet season of the eastern edge of the southern Amazon. All piControl runs show a strong wet bias compared to observations in this southeastern Amazon region (Figure S1), so the change in rainfall might not be accurate;

(iii) in Africa, the WAM region is where the largest changes occur, with a longer dry season and a shorter wet season, especially at the southern edge of the Sahel. There is negligible change in the dry season monthly precipitation (which was already close to zero), but there is a reduction in the wet season precipitation. The only outlier is the Congo region, which benefits from a a shorter dry season and a longer (but drier) wet season due to the southward shift of the Atlantic ITCZ;

(iv) for the ISM, the drying is more predominant in the wet season. While the dry season is longer by up to one month inland, the wet season is shorter by at least a month almost everywhere and has significantly drier months in the north-east;

(v) the EASM has a mixed change in the dry season: the northern part has a longer and the southern a shorter dry season, with little change in the average precipitation. The overall drying is more drastic in the wet season, similarly to the ISM, with an overall shorter wet season and drier months.

3 Discussion and Conclusions

The four monsoon systems investigated in this work are vital parts of the global climate. Nearly three-quarters of the world's population is affected by monsoons, making them a high priority regarding possible impacts of anthropogenic global warming. This work is the first one to compare the effect of an AMOC collapse on monsoon systems in multiple CMIP6 GCM experiments which apply the same hosing scenario.

While the four models used in this study have different Atlantic ITCZ biases (Figure S3), their agreement on the pattern of the precipitation response to an AMOC collapse (Figures 2, S5 and S6 and Tables S2 and S3) is a strong case for the robustness of that pattern (Figures 1 and 3).

The overall response structures are remarkably consistent across models, both geographically and seasonally (Figure S5). The WAM, ISM and EASM show an overall drying with a shorter wet season and longer dry season in response to an AMOC collapse. The SAM shows a more spatially dependant pattern, with an overall annual increase in rainfall, a higher increase of annual precipitation and shorter dry season in the south and less pronounced change in the north.

The year-long reduction in precipitation associated with WAM, ISM and EASM would likely have severe ecological and socio-economic impacts. The effect of an AMOC collapse on the SAM and, hence, on the Amazon rainforest, is more uncertain. (Parsons et al., 2014) showed that even with an overall decrease in yearly rainfall sums over the region, a shorter dry season leads to increased productivity in the Amazon rainforest. However, the effect on the SAM dry season shown in this work is complex: in the northern Amazon, there is a shift of the seasonal cycle to later in the year in all models, and also an increase in dry season length. To understand the effect this would have on the rainforest requires additional modelling considering the vegetation response. On the other hand, the effect on the southern Amazon is different: more overall rainfall and a shortened and wetter dry season. This southern Amazon region is also the one shown to be losing resilience faster in the past decades (Boulton et al., 2022) and therefore may be more susceptible to changes in rainfall. This relative complexity in Amazon rainfall response may be the reason for the contrasting results of past models (Stouffer et al., 2006; Jackson et al., 2015) with regards to the effect of an AMOC collapse on the Amazon. The agreement of four different GCM experiments allows us to conclude that the overall effect of an AMOC collapse on the Amazon could counteract precipitation reductions projected for future global warming scenarios (see Arias et al. (2021)).

This work presents the effects of an AMOC collapse in tropical monsoon systems, inferred from simulations of the NAHosMIP project. Detailed analyses of many of the relevant physical processes at play in the models have already been presented in works on earlier hosing experiments, and have been identified in our results (Orihuela-Pinto et al., 2022; Good et al., 2021; Chang et al., 2008; Yu et al., 2009).

There is considerable uncertainty in the impact future global warming will have on monsoon rainfall (Arias et al., 2021; Wang et al., 2021; Moon & Ha, 2020). We show that our models agree much more for AMOC hosing experiments than they do for other CMIP6 warming experiments. Our work thus allows us to constrain projections in this high-uncertainty region.

The key property of the impacts discussed in this work is that they are practically irreversible. Whilst the direct impacts on monsoon rainfall from anthropogenic forcing could be reversed if the temperature is returned to pre-industrial levels, the collapse of the AMOC is permanent in the experiments considered in this study, something that was not certain in many previous hosing experiments. The impacts presented in this work could thus represent practically irreversible long-term changes that would persist even after a return to pre-industrial conditions.

Regardless of whether or not it is combined with increased temperatures, an AMOC collapse would result in a major rearranging of the global monsoon systems. This work shows that this rearrangement will have unfavorable effects on the WAM, ISM and EASM and a more uncertain effect on the SAM and the Amazon rainforest.

Methods

Model runs and processing of the outputs

We use the uniform hosing experiments from the North Atlantic Hosing Model Intercomparison study (NAHosMIP, Jackson et al. (2022)). These experiments start from the respective pre-industrial control (piControl) runs of CMIP6 models, and apply a 0.3Sv uniform hosing from 50°N to the Bering Strait. This hosing is applied for a given length of time and then stopped, after which the model continues to run. In the models we consider, the AMOC remains in the weak state after the hosing is turned off. For HadGEM, CanESM and CESM, we use the u03-r50 experiments, in which the hosing has been halted after 50 years. For IPSL, we use the u03-r100 experiments, in which the hosing has been halted after 100 years.

For consistent comparison we use 80 years from each of the different model runs. As the AMOC takes a few years to settle into a stable state after the hosing is turned off, we take the last 80 years from HadGEM and CanESM, years 100-180 from CESM and years 60-140 from IPSL. For all models we use the first 80 years from the piControl.

For the comparison with the observational GPCP dataset the model outputs are regridded to a regular 2.5° grid. For calculation of the ensemble mean the model outputs are regridded to the coarsest-resolution model grid, that of the CanESM5 model. When correlating the HadGEM3-GM3-1MM output with the other three models, the HadGEM outputs are regridded to the respective model grid. All regridding is done using a first order conservative remapping.

4xCO2 experiments are taken from the CMIP6 abrupt-4xCO2 experiments, where an instantaneous quadrupling of the pre-industrial atmospheric CO_2 concentration is imposed and this concentration is kept constant. As the AMOC takes a few years to react to this we take years 60-140 from all models, using 80 years for consistent comparison with the NAHosMIP runs. We also use the CMIP6 historical runs, in which the anthropogenic forcings of 1850-2014 are applied to the climate, starting from some point in the piControl run. For all models, the r1i1p1f1 ensemble member is used, with the exception of HadGEM3, for which r1i1p1f3 is used. This is also the case for the piControl and 4xCO2 runs.

For the scenario-mip CMIP6 runs ssp585 and ssp126 we use years 2080-2100 for consistency across models. The same ensemble members are used as above, except for CESM2 where we use r4i1p1f1 in ssp126 and r10i1p1f1 in ssp585.

Observational Datasets

For comparison with model results and calculation of the ITCZ latitude (which requires precipitation data over land and sea), we use the GPCP Precipitation data provided by NOAA/OAR/ESRL PSL, Boulder, Colorado, USA (Adler et al., 2018) available for 1979-2020. For all other precipitation analyses we use the GPCC Full Data Monthly Product Version 2020 at 0.25° from 1921 to 2019 (the first 20 years are not used due to the paucity of measurements in the regions of interest) (Schneider et al., 2020).

For the observed AMOC strength (Figure S4) the RAPID AMOC monitoring project data is used (Frajka-Williams et al., 2021).

ITCZ calculation

The ITCZ latitude is calculated following Good et al. (2021) to evaluate the model performance and effect of AMOC collapse.

The Atlantic ITCZ latitude is calculated in the area 35–15°W 15°S–15°N as a precipitation-weighted mean, as follows:

$$\phi_{itcz} = \sum_i \frac{\mathrm{P}_{35-15^\circ W,\phi_i} \cdot \phi_i}{\mathrm{P}_{35-15^\circ W,15^\circ S-15^\circ N}} \tag{1}$$

Where $\mathrm{P}_{35-15^\circ W,\phi_i}$ is the zonally averaged precipitation at latitude ϕ_i, and $\mathrm{P}_{35-15^\circ W,15^\circ S-15^\circ N}$ is the precipitation averaged over the whole region. Each latitude is thus weighted by the precipitation at that latitude.

The same procedure is repeated in the Indian and Pacific oceans for the following areas: 55°E-95°E, 15°S-15°N and 120°E-95°W,15°S-15°N, respectively.

The ITCZ and AMOC strength in the different models

When compared to the observed seasonal cycle of the Atlantic ITCZ (hereafter simply ITCZ) the models can be divided into two groups (Figure S3 (a)-(d)): (i) The CanESM and IPSL piControl runs have ITCZ latitudes going much further south (around 8°) in the December – March season (DJFM) than in observations. Their ITCZ varies more than 13° in latitude in a year, whilst the change in the average ITCZ seasonal cycle in the observation is 8.5 °. It turns out that these two models only have a small ($\leq 1°$) latitudinal shift in the ITCZ between the control and weak AMOC; (ii) HadGEM and CESM have a more realistic seasonal cycle of the ITCZ latitude, where the southward bias of the piControl is about 1 ° for all months. Compared to the Atlantic Ocean, the biases in simulated ITCZ latitudes in the piControl run relative to the observations are smaller in the Indian and Pacific Oceans (see Fig S8).

On the other hand, those models which have a more realistic latitudinal shift are also those which have a stronger piControl AMOC at 26.5N: In CanESM and IPSL the piControl AMOC has a strength of 11.27 Sv and 12.49 Sv respectively, and a post-hosing weak AMOC of 6.53 Sv and 5.20 Sv (Figure S4). HadGEM and CESM, on the other hand, have a much stronger piControl AMOC at 16.46 Sv and 17.39, respectively, and a post-hosing AMOC at 5.82 Sv and 8.70 Sv. The RAPID array obsevational measurements of the AMOC strength at 26.5N have a mean of 16.9 ± 4.6 Sv in 2004-2020 (Frajka-Williams et al., 2021), closer to HadGEM and CESM than to the other two models. Note, however, that these are historical observations and thus include the effect of anthropogenic forcings, and cannot be directly compared with the piControl simulations.

However although the collapsed AMOC has a similar strength in all four models, there are still major differences between the post-collapsed ITCZ cycles of the two groups of models. It is more likely that other properties of the IPSL and CanESM models cause both an extended ITCZ excursion to the south and a weaker piControl AMOC. In the CMIP6 Atmospheric Model Intercomparison Project (AMIP) experiments CanESM and IPSL have a seasonal ITCZ cycle much closer to the observations, without the southward excursion (Fig S9). As the AMIP models are forced with historical SSTs, the biases in the piControl runs of CanESM and IPSL are likely due to either biases in the modelled SST fields or in the SST-precipitation interactions in these models. Note, however, that the AMIP models include historical forcings which are absent in the piControl runs. Thus, for a reliable estimate of the magnitude (and not only the sign) of the precipitation change due to an AMOC collapse, further work should focus on the differences in the AMOC and SST biases of the different models.

Defining dry and wet seasons

The dry and wet seasons are defined using a non-parametric approach for consistency across monsoon regions. First, percentile boundaries are calculated for each region using all gridpoints and years. The dry or wet season months in a given year and gridpoint are then all the months that have less or more rain than the chosen percentile boundary of the region. The 40th and 60th percentile are chosen for the dry and wet season, respectively. The dry season percentile is chosen such that for the SAM the dry season monthly rainfall limit is about 100 mm, which is the mean monthly evapotranspiration value of tropical forests (below this value evapotranspiration exceeds rainfall, see (Carvalho et al., 2021)).

The averaged dry (wet) season length is then the mean of dry (wet) season length over all years. The total dry (wet) season precipitation is, accordingly, the sum of rainfall in all months of the season, which is again averaged over all years to give the average total dry (wet) season precipitation. However, when comparing seasonal rainfall across runs with different season lengths, the total precipitation will be biased by the difference in season length. An average dry (wet) season monthly precipitation value is therefore defined by dividing the total dry (wet) season rainfall in a year by the length of the dry (wet) season in that year, and the average is calculated as

$$p_{i,\text{dry,avg}} = \frac{1}{T}\sum_{t=1}^{T}\frac{p_{i,t,\text{dry}}}{x_{i,t,\text{dry}}}\,, \tag{2}$$

where $p_{i,t,\text{dry}}$ and $x_{i,t,\text{dry}}$ are respectively the total dry season precipitation and dry season length in grid-point i in year t, and the sum is over all years T.

When comparing these values between the piControl and weak AMOC model runs, there are two ways to define the dry (wet) season for the weak AMOC run. The first is to use the regions' percentile boundary values calculated for the piControl run, and apply them as the limit defining the weak AMOC seasons. The second is to independently calculate new percentiles for the weak AMOC precipitation and use those as the defining limits. The first option reflects the experience of an abrupt change in the AMOC, as it shows how the "known" seasons would change after a collapse. The second is more applicable to an analysis of a long-term state, as it shows what the dry (wet) season would look like in a world with a weak AMOC. As we are interested in the effect of an abrupt collapse on ecosystems and societies which are in general adapted to a given pattern and strength of seasonal rainfall, the value of interest will be the first one, which reflects how the known seasons would change.

Model bias

Figure S1 shows the difference between the piControl run for the four models and the global GPCP observations. The pattern in the yearly average precipitation bias is as follows: (i) For the SAM all models except HadGEM show an ∼2mm/day dry bias, whilst HadGEM shows a weak wet bias in the southern Amazon and a weak dry bias in the northern Amazon; (ii) For the WAM there is a small dry bias in all four models; (iii) For the ISM HadGEM and CanESM have a dry bias everywhere, whilst CESM and IPSL have a dry bias in the north and a wet bias in the south; (iv) For the EASM all models except IPSL have a wet bias, whilst IPSL has a small dry bias. The piControl run is the starting point with which we compare the collapsed AMOC state, so although the observations are historical and thus include anthropogenic forcings not present in the piControl runs, these comparisons are still informative.

Agreement between HadGEM3-GC3-1MM and other models

In Figure 5 the changes in dry and wet seasons are shown only for HadGEM. This model was chosen due to its realistic Atlantic ITCZ and its higher spatial resolution. To justify the use of HadGEM as representative of all models, Figure S7 shows the regions in which all three other models or two of the other three models show the same sign of precipitation anomaly as HadGEM, and Table S5 shows the correlation of the other models with HadGEM. These figures show the remarkable agreement between the models. The only region in the monsoon areas of interest where HadGEM does not agree with the other models is in the northeastern Amazon, where HadGEM shows a slight overall drying. However, it can be seen that the detailed seasonal response of precipitation in that region is the same in all four models (Figure 4). The annual mean in this region is the combined effect of a drying in January to June and increased rainfall in the rest of the year. It is likely that the dry region in HadGEM has a different ratio between these two effects than in the other models, but in practice has a similar response.

4 Open Research

The NAHosMIP model data is available at https://doi.org/10.5281/zenodo.7324394. The pre-industrial control, 4xCO2 and AMIP experimental data is available via the Earth System Grid Federation (ESGF) servers with information on obtaining data available from https://pcmdi.llnl.gov/CMIP6/Guide/dataUsers.html. The GPCP and GPCC precipitation datasets are available at https://psl.noaa.gov/. The RAPID observational data is available at https://rapid.ac.uk/. All code used to analyse the data and generate figures will be uploaded at https://github.com/mayaby.

Acknowledgments

MBY and NB acknowledge funding by the European Union's Horizon 2020 research and innovation programme under the Marie Sklodowska-Curie grant agreement No.956170. NB acknowledges funding by the Volkswagen foundation. NB and LCJ acknowledge funding by the TiPES project. This is TiPES contribution #X; the TiPES ('Tipping Points in the Earth System') project has received funding from the European Union's Horizon 2020 research and innovation programme under grant agreement No. 820970. NB acknowledges further funding by the German Federal Ministry of Education and Research under grant No. 01LS2001A. OS thanks the CCCma team for support. LCJ was supported by the Met Office Hadley Centre Climate Programme funded by BEIS and Defra (grant GA01101).

References

Adler, R. F., Sapiano, M. R. P., Huffman, G. J., Wang, J.-J., Gu, G., Bolvin, D., … Shin, D.-B. (2018). The global precipitation climatology project (gpcp) monthly analysis (new version 2.3) and a review of 2017 global precipitation. *Atmosphere*, *9*(4). Retrieved from https://www.mdpi.com/2073-4433/9/4/138 doi: 10.3390/atmos9040138

Arias, P. A., Bellouin, N., Coppola, E., Jones, R. G., Krinner, G., Marotzke, J., … Zickfeld, K. (2021). Technical summary [Book Section]. In V. Masson-Delmotte et al. (Eds.), *Climate change 2021: The physical science basis. contribution of working group i to the sixth assessment report of the intergovernmental panel on climate change* (chap. 1). Cambridge, United Kingdom and New York, NY, USA: Cambridge University Press. Retrieved from https://www.ipcc.ch/report/ar6/wg1/downloads/report/IPCC_AR6_WGI_TS.pdf

Boers, N. (2021). Observation-based early-warning signals for a collapse of the Atlantic Meridional Overturning Circulation. *Nature Climate Change*, *11*(8), 680–688. Retrieved from http://dx.doi.org/10.1038/s41558-021-01097-4 doi: 10.1038/s41558-021-01097-4

Boulton, C. A., Lenton, T. M., & Boers, N. (2022). Pronounced loss of Amazon rainforest resilience since the early 2000s. *Nature Climate Change*, *12*(March). doi: 10.1038/s41558-022-01287-8

Caesar, L., McCarthy, G. D., Thornalley, D. J., Cahill, N., & Rahmstorf, S. (2021). Current Atlantic Meridional Overturning Circulation weakest in last millennium. *Nature Geoscience*, *14*(3), 118–120. Retrieved from http://dx.doi.org/10.1038/s41561-021-00699-z doi: 10.1038/s41561-021-00699-z

Carvalho, N. S., Anderson, L. O., Nunes, C. A., Pessôa, A. C., Silva Junior, C. H., Reis, J. B., … Aragão, L. E. (2021). Spatio-Temporal variation in dry season determines the Amazonian fire calendar. *Environmental Research Letters*, *16*(12). doi: 10.1088/1748-9326/ac3aa3

Chang, P., Zhang, R., Hazeleger, W., Wen, C., Wan, X., Ji, L., … Seidel, H. (2008). Oceanic link between abrupt changes in the north Atlantic ocean and the African monsoon. *Nature Geoscience*, *1*(7), 444–448. doi: 10.1038/ngeo218

Drijfhout, S. S., Weber, S. L., & van der Swaluw, E. (2011). The stability of the MOC as diagnosed from model projections for pre-industrial, present and future climates. *Climate Dynamics*, *37*(7-8), 1575–1586. doi: 10.1007/s00382-010-0930-z

Frajka-Williams, E., Moat, B., Smeed, D., Rayner, D., Johns, W., Baringer, M., …

Collins, J. (2021). *Atlantic meridional overturning circulation observed by the rapid-mocha-wbts (rapid-meridional overturning circulation and heatflux array-western boundary time series) array at 26n from 2004 to 2020 (v2020.1).* doi: 10.5285/cc1e34b3-3385-662b-e053-6c86abc03444

Good, P., Boers, N., Boulton, C. A., Lowe, J. A., & Richter, I. (2021). How might a collapse in the Atlantic Meridional Overturning Circulation affect rainfall over tropical South America? *Climate Resilience and Sustainability*(November), 1–13. doi: 10.1002/cli2.26

Häggi, C., Chiessi, C. M., Merkel, U., Mulitza, S., Prange, M., Schulz, M., & Schefuß, E. (2017). Response of the Amazon rainforest to late Pleistocene climate variability. *Earth and Planetary Science Letters*, *479*, 50–59. Retrieved from http://dx.doi.org/10.1016/j.epsl.2017.09.013 doi: 10.1016/j.epsl.2017.09.013

Henry, L. G., McManus, J. F., Curry, W. B., Roberts, N. L., Piotrowski, A. M., & Keigwin, L. D. (2016). North Atlantic ocean circulation and abrupt climate change during the last glaciation. *Science*, *353*(6298), 470–474. doi: 10.1126/science.aaf5529

Jackson, L. C., Asenjo, E. A. D., Bellomo, K., Danabasoglu, G., Haak, H., Hu, A., ... Swingedouw, D. (2022). Understanding AMOC stability : the North Atlantic Hosing Model Intercomparison Project. *Geoscientific Model Development Discussions*(November), 1–32. Retrieved from https://gmd.copernicus.org/preprints/gmd-2022-277/ doi: 10.5194/gmd-2022-277

Jackson, L. C., Kahana, R., Graham, T., Ringer, M. A., Woollings, T., Mecking, J. V., & Wood, R. A. (2015). Global and European climate impacts of a slowdown of the AMOC in a high resolution GCM. *Climate Dynamics*, *45*(11-12), 3299–3316. Retrieved from http://dx.doi.org/10.1007/s00382-015-2540-2 doi: 10.1007/s00382-015-2540-2

Jackson, L. C., & Wood, R. A. (2018). Hysteresis and Resilience of the AMOC in an Eddy-Permitting GCM. *Geophysical Research Letters*, *45*(16), 8547–8556. doi: 10.1029/2018GL078104

Lee, J. Y., Marotzke, J., Bala, G., Cao, L., Corti, S., Dunne, J. P., ... Zhou, T. (2021). Future global climate: Scenario-based projections and near-term information [Book Section]. In V. Masson-Delmotte et al. (Eds.), *Climate change 2021: The physical science basis. contribution of working group i to the sixth assessment report of the intergovernmental panel on climate change* (chap. 4). Cambridge, United Kingdom and New York, NY, USA: Cambridge University Press. Retrieved from https://www.ipcc.ch/report/ar6/wg1/downloads/report/IPCC_AR6_WGI_Chapter_04.pdf

Liu, W., Xie, S. P., Liu, Z., & Zhu, J. (2017). Overlooked possibility of a collapsed atlantic meridional overturning circulation in warming climate. *Science Advances*, *3*(1), 1–8. doi: 10.1126/sciadv.1601666

Liu, Y., Chiang, J. C., Chou, C., & Patricola, C. M. (2014). Atmospheric teleconnection mechanisms of extratropical North Atlantic SST influence on Sahel rainfall. *Climate Dynamics*, *43*(9-10), 2797–2811. doi: 10.1007/s00382-014-2094-8

Marzin, C., Kallel, N., Kageyama, M., Duplessy, J. C., & Braconnot, P. (2013). Glacial fluctuations of the Indian monsoon and their relationship with North Atlantic climate: New data and modelling experiments. *Climate of the Past*, *9*(5), 2135–2151. doi: 10.5194/cp-9-2135-2013

Moon, S., & Ha, K. J. (2020). Future changes in monsoon duration and precipitation using CMIP6. *npj Climate and Atmospheric Science*, *3*(1), 1–7. Retrieved from http://dx.doi.org/10.1038/s41612-020-00151-w doi: 10.1038/s41612-020-00151-w

Mosblech, N. A., Bush, M. B., Gosling, W. D., Hodell, D., Thomas, L., Van Calsteren, P., ... Van Woesik, R. (2012). North Atlantic forcing of Amazonian precipitation during the last ice age. *Nature Geoscience*, *5*(11), 817–820. doi: 10.1038/ngeo1588

Orihuela-Pinto, B., England, M. H., & Taschetto, A. S. (2022). Interbasin and interhemispheric impacts of a collapsed Atlantic Overturning Circulation. *Nature Climate Change*. doi: 10.1038/s41558-022-01380-y

Parsons, L. A., Yin, J., Overpeck, J. T., Stouffer, R. J., & Malyshev, S. (2014). Influence of the atlantic meridional overturning circulation on the monsoon rainfall and carbon balance of the American tropics. *Geophysical Research Letters*, *41*(1), 146–151. doi: 10.1002/2013GL058454

Rahmstorf, S. (2002). NAT(419,207)-circulation. , *419*(September), 207–214.

Rahmstrof, S., Crucifix, M., Ganopolski, A., Goosse, H., Kamenkovich, I., Knutti, R., ... Weaver, A. J. (2005). Thermohaline circulation hysteresis: A model intercomparison. *Geophysical Research Letters*, *32*(23), 1–5. doi: 10.1029/2005GL023655

Romanou, A., Rind, D., Jonas, J., Miller, R., Kelley, M., Russell, G., ... Schmidt, G. A. (2023). Stochastic Bifurcation of the North Atlantic Circulation Under A Mid-Range Future Climate Scenario With The NASA-GISS ModelE. *Journal of Climate*, 1 - 49. Retrieved from `https://journals.ametsoc.org/view/journals/clim/aop/JCLI-D-22-0536.1/JCLI-D-22-0536.1.xml` doi: 10.1175/JCLI-D-22-0536

Sandeep, N., Swapna, P., Krishnan, R., Farneti, R., Prajeesh, A. G., Ayantika, D. C., & Manmeet, S. (2020). South Asian monsoon response to weakening of Atlantic meridional overturning circulation in a warming climate. *Climate Dynamics*, *54*(7-8), 3507–3524. Retrieved from `https://doi.org/10.1007/s00382-020-05180-y` doi: 10.1007/s00382-020-05180-y

Schneider, U., Becker, A., Finger, P., Rustemeier, E., & Ziese, M. (2020). *Gpcc full data monthly product version 2020 at 0.25°: Monthly land-surface precipitation from rain-gauges built on gts-based and historical data.* doi: 10.5676/DWD_GPCC/FD_M_V2020_025

Stommel, H. (1961). Thermohaline Convection with Two Stable Regimes of Flow. *Tellus*, *13*(2), 224–230. doi: 10.3402/tellusa.v13i2.9491

Stouffer, R. J., Yin, J., Gregory, J. M., Dixon, K. W., Spelman, M. J., Hurlin, W., ... Weber, S. L. (2006). Investigating the causes of the response of the thermohaline circulation to past and future climate changes. *Journal of Climate*, *19*(8), 1365 - 1387. Retrieved from `https://journals.ametsoc.org/view/journals/clim/19/8/jcli3689.1.xml` doi: https://doi.org/10.1175/JCLI3689.1

Sun, Y., Clemens, S. C., Morrill, C., Lin, X., Wang, X., & An, Z. (2012). Influence of Atlantic meridional overturning circulation on the East Asian winter monsoon. *Nature Geoscience*, *5*(1), 46–49. doi: 10.1038/ngeo1326

Wang, B., Biasutti, M., Byrne, M. P., Castro, C., Chang, C. P., Cook, K., ... Zhou, T. (2021). Monsoons climate change assessment. *Bulletin of the American Meteorological Society*, *102*(1), E1-E19. doi: 10.1175/BAMS-D-19-0335.1

Wassenburg, J. A., Vonhof, H. B., Cheng, H., Martínez-García, A., Ebner, P. R., Li, X., ... Haug, G. H. (2021). Penultimate deglaciation Asian monsoon response to North Atlantic circulation collapse. *Nature Geoscience*, *14*(12), 937–941. doi: 10.1038/s41561-021-00851-9

WRCP, W. C. R. P. (n.d.). *The global monsoon systems.* Retrieved from `https://www.wcrp-climate.org/documents/monsoon_factsheet.pdf`

Yu, L., Gao, Y. Q., Wang, H. J., Guo, D., & Li, S. L. (2009). The responses of East Asian Summer monsoon to the North Atlantic Meridional Overturning Circulation in an enhanced freshwater input simulation. *Chinese Science Bulletin*, *54*(24), 4724–4732. doi: 10.1007/s11434-009-0720-3

Supporting Information for "Robust and irreversible impacts of an AMOC collapse on tropical monsoon systems: a multi-model comparison"

M. Ben-Yami[1,2], P. Good[3], L. C. Jackson [3], M. Crucifix [4], A. Hu [5], O. Saenko [6], D. Swingedouw [7]and N. Boers [1,2,8]

[1]Earth System Modelling, School of Engineering and Design, Technical University of Munich, Munich, Germany

[2]Potsdam Institute for Climate Impact Research, Potsdam, Germany

[3]Met Office, Exeter, UK

[4]Earth and Life Institute, UCLouvain, Place Louis Pasteur 3, Louvain-La-Neuve, 1348, Belgium

[5]Climate and Global Dynamics Lab, National Center for Atmospheric Research, Boulder, CO 80307, USA

[6]SEOS, University of Victoria, BC, Canada

[7]Environnements et Paléoenvironnements Océaniques et Continentaux (EPOC)— Université de Bordeaux, Pessac, France

[8]Department of Mathematics and Global Systems Institute , University of Exeter, Exeter, UK

Contents of this file

Region	Longitude		Latitude	
	Min	Max	Min	Max
AM south	-75	-42.5	-15	-5
AM north	-75	-55	-5	5
WAM	-20	25	5	20
ISM	70	85	5	25
EASM	110	140	10	40

Table S1. Coordinates used to define the tropical monsoon boxes for Figure 4.

Region	Hosing	4xCO2	SSP585	SSP126
Global	0.66	0.65	0.66	0.60
60S-60N	0.66	0.57	0.58	0.51
Extratropics	0.49	0.74	0.68	0.62
Tropics	0.64	0.40	0.53	0.40
Southern AM	0.79	0.15	0.27	0.03
Northern AM	0.18	0.68	0.61	0.36
WAM	0.99	0.15	0.48	0.24
ISM	0.95	0.75	0.80	0.74
EASM	0.71	0.73	0.96	0.70

Table S2. Values from Figure 2a. Fraction of gridpoints in the respective region land areas where all four models of the experiments agree on the sign of mean annual precipitation anomaly. Extratropics are defined as 20S-60S and 20N-60N, and the tropics as 20S-20N, and the last five regions are as defined in Table S1. For the tropics and most monsoon regions there is more agreement in the hosing experiment than in the other experiments.

Region	Hosing	4xCO2	SSP585	SSP126
Global	0.35	0.52	0.49	0.33
60S-60N	0.42	0.41	0.39	0.26
Extratropics	0.33	0.56	0.49	0.33
Tropics	0.40	0.31	0.30	0.21
Southern AM	0.60	0.05	0.09	0.08
Northern AM	0.73	0.32	0.30	0.15
WAM	0.65	0.17	0.21	0.13
ISM	0.44	0.30	0.34	0.12
EASM	0.26	0.50	0.36	0.21

Table S3. Values from Figure 2b. Fraction of months in the respective region land areas where all four models of the experiments agree on the sign of mean monthly precipitation anomaly. Extratropics are defined as 20S-60S and 20N-60N, and the tropics as 20S-20N, and the last five regions are as defined in Table S1. For the tropics and most monsoon regions there is more agreement in the hosing experiment than in the other experiments.

Region	Longitude		Latitude	
	Min	Max	Min	Max
AM	-85	-30	-20	11
WAM	-20	35	-10	25
ISM	70	85	5	25
EASM	110	140	10	40

Table S4. Coordinates used to define the tropical monsoon regions for calculation of the dry and wet season in Figure 5.

Region	CanESM5			CESM2			IPSL		
	Cont	Weak	Diff	Cont	Weak	Diff	Cont	Weak	Diff
AM	0.59	0.83	0.68	0.54	0.74	0.67	0.69	0.84	0.69
WAM	0.90	0.93	0.88	0.91	0.88	0.88	0.81	0.90	0.77
ISM	0.81	0.85	0.62	0.89	0.88	0.65	0.39	0.47	-0.09
EASM	0.82	0.81	0.73	0.83	0.86	0.75	0.44	0.16	-0.00

Table S5. Correlation of precipitation of the CanESM5, CESM2, and IPSL models with HadGEM. The table shows Pearson's correlation coefficient of the time-averaged precipitation patterns in the four regions between HadGEM and the three other models, for the piControl (Cont) and weak AMOC (Weak) runs, as well as the difference between them (Diff). The regions are defined as in Figure 5.

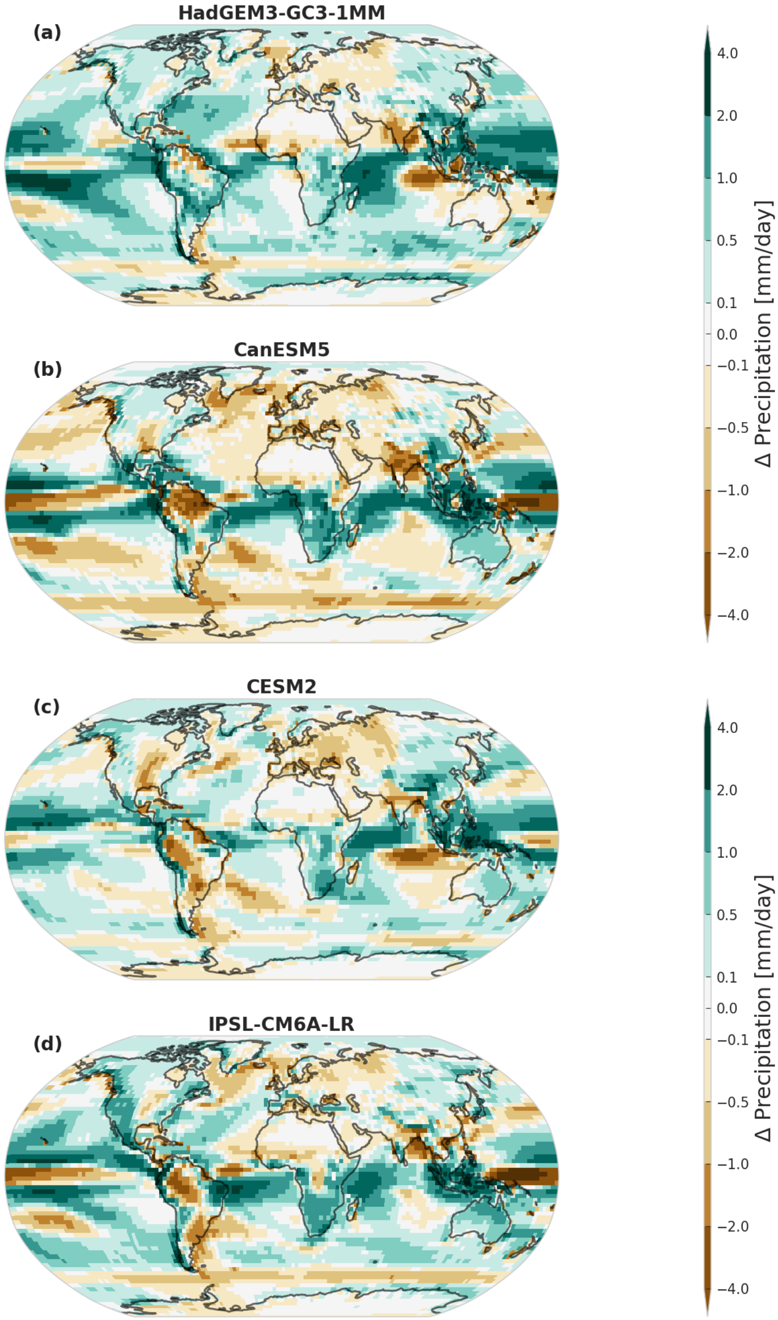

Figure S1. Average precipitation bias (piControl run minus GPCP observations) for the four models: a. HadGEM3, b. CanESM, c. CESM, and d. IPSL. The bias can be as large as the effect of an AMOC collapse over the monsoon regions. In general there is a dry bias over the ISM, wet bias for the EASM and a small dry bias for the WAM. However there is no monsoon region where all models have the same bias, and for the SAM especially they all exhibit distinct patterns. Note that the observational period includes historical forcings which are not present in the piControl.

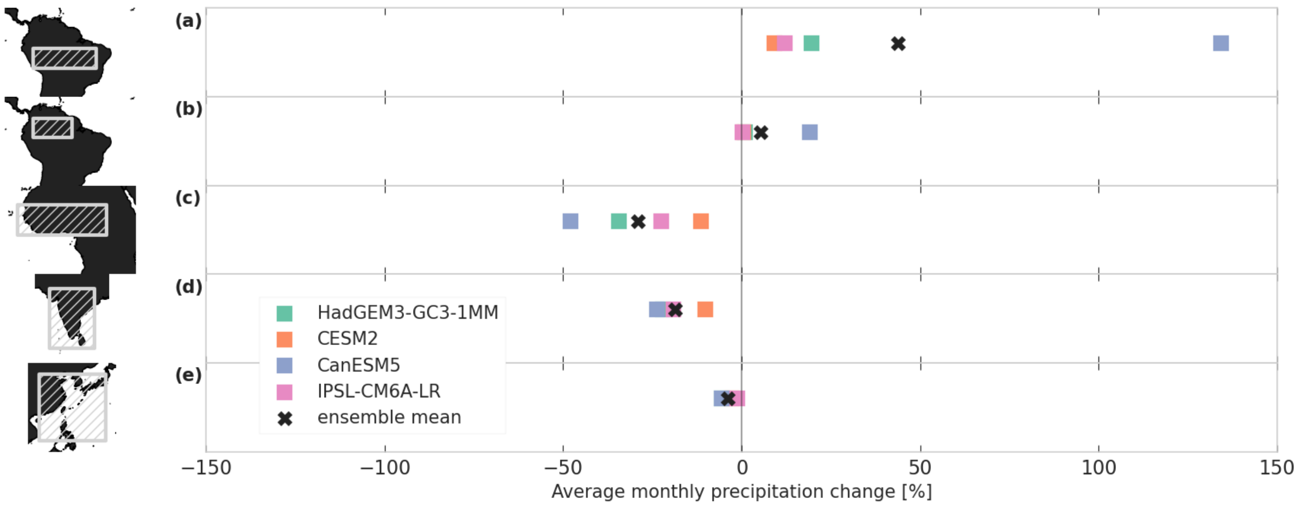

Figure S2. The percentage rainfall change in the land area of five monsoon regions. The first column shows the region for which the precipitation difference is averaged: two parts of the SAM (a,b), as well as in the WAM (c), ISM (d), and EASM (e) (see Table S1). For each model, the x-axis is the average of the 12 individual mean monthly precipitation percentage changes in the region. As well as for the four models (coloured square markers), the ensemble mean is shown (black cross).

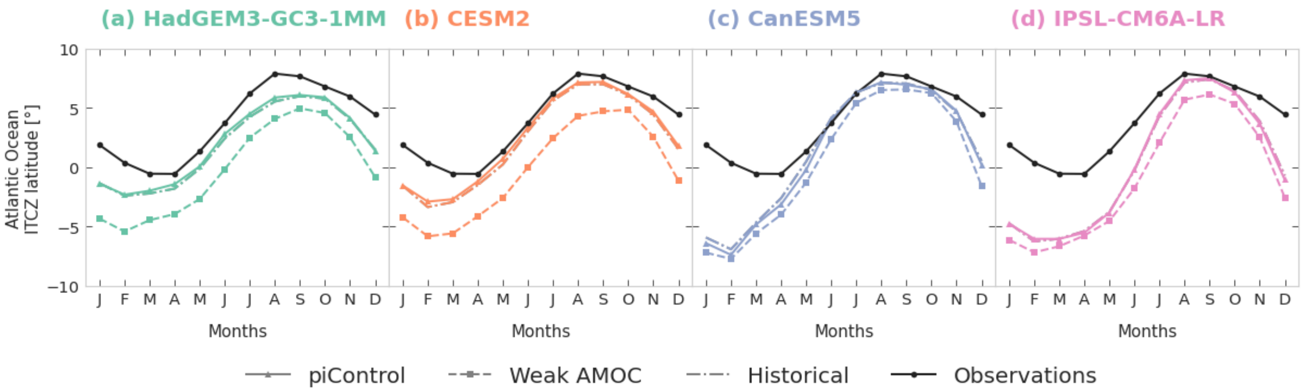

Figure S3. The mean location of the Atlantic ITCZ for each month of the year, before/after AMOC collapse. The observational data is shown in black, the piControl model output in thick coloured lines, the historical runs in dot-dashed coloured lines, and the weak AMOC model output in dashed coloured lines, for a. HadGEM3, b. CanESM, c. CESM, and d. IPSL. See Methods for details.

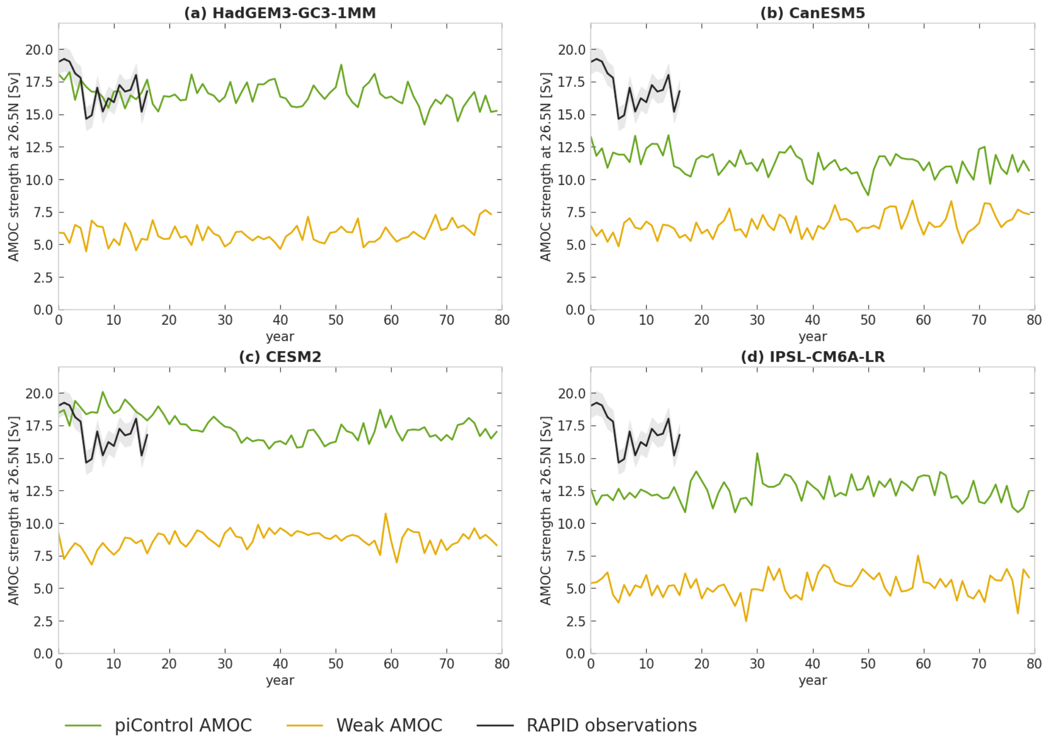

Figure S4. Yearly average AMOC strength at 26.5N for the four model experiments: a. HadGEM3, b. CanESM, c. CESM, and d. IPSL. The piControl strength is shown in solid green and the post-hosing AMOC strength in solid gold. The 4xCO2 AMOC strength is shown in dashed brown. Only the 80 years used in this work are shown. For comparison the RAPID array of AMOC observational measurements from 2004 to 2020 are shown in black with a ±0.9 Sv uncertainty shading. Note, however, that these are historical observations and thus include the effect of anthropogenic forcings, and cannot be directly compared with the piControl simulations. The piControl AMOC is stronger in HadGEM and CESM at about 18 Sv, whilst both CanESM and IPSL have a weaker AMOC at about 12 Sv. The collapsed, weak AMOC has a similar strength in all four models, about 6 Sv, except in CESM2 where its strength is about 8.7 Sv. The 4xCO2 amoc is about the same strength as the collapsed AMOC, except in CESM2 where it is about 2 Sv weaker.

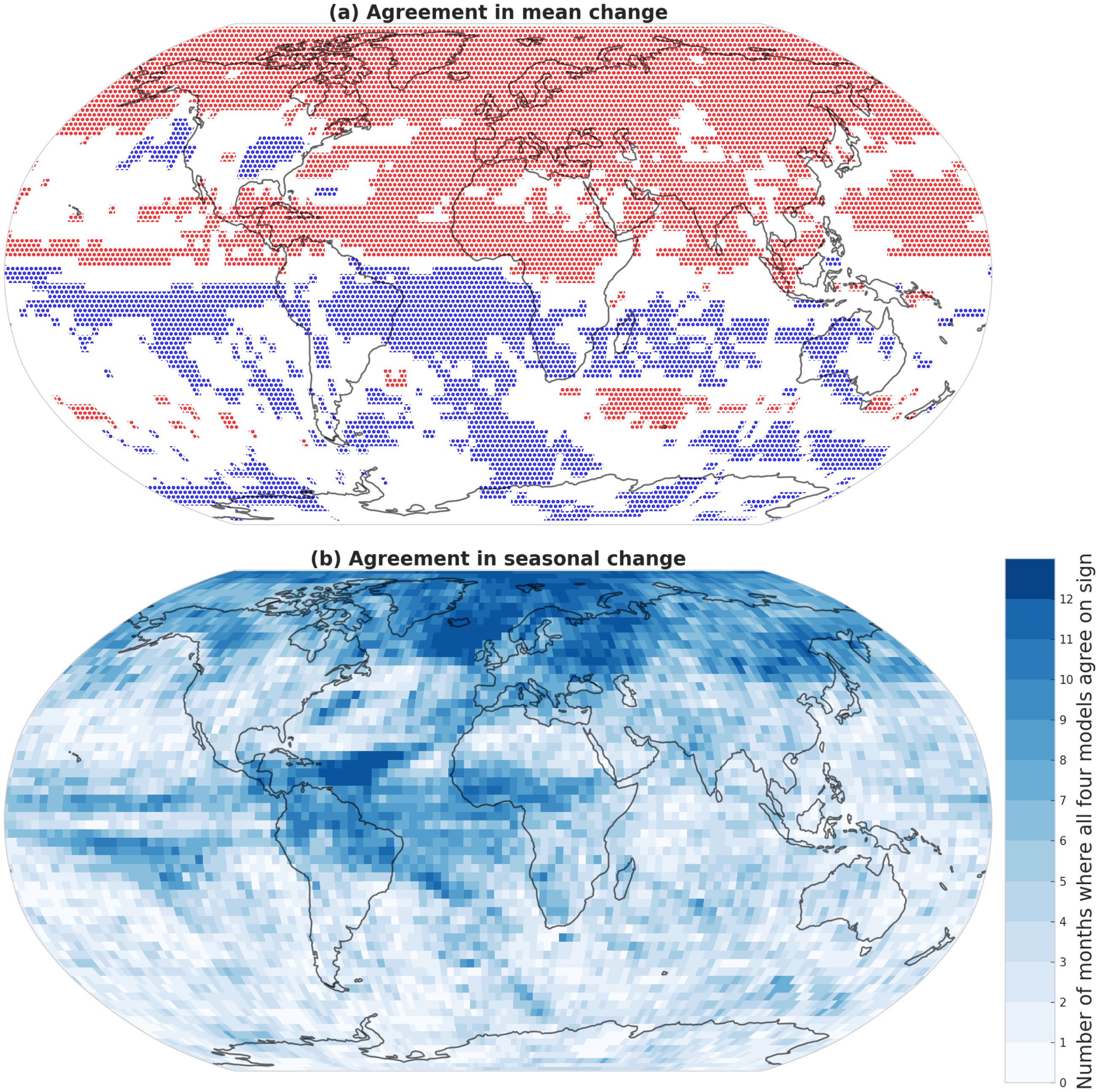

Figure S5. Model agreement in NAHosMIP. (a) The red (blue) stippling indicates the grid-points where all four models agree on the negative (positive) sign of mean annual precipitation anomaly when the hosing experiment is compared with the piControl run. (b) The figures are colored according to the number of months in which the change in the mean monthly rainfall relative to the piControl mean agrees in sign in all four model runs. There is high agreement in the hosing experiments for the SAM and WAM and moderate agreement for the ISM and EASM.

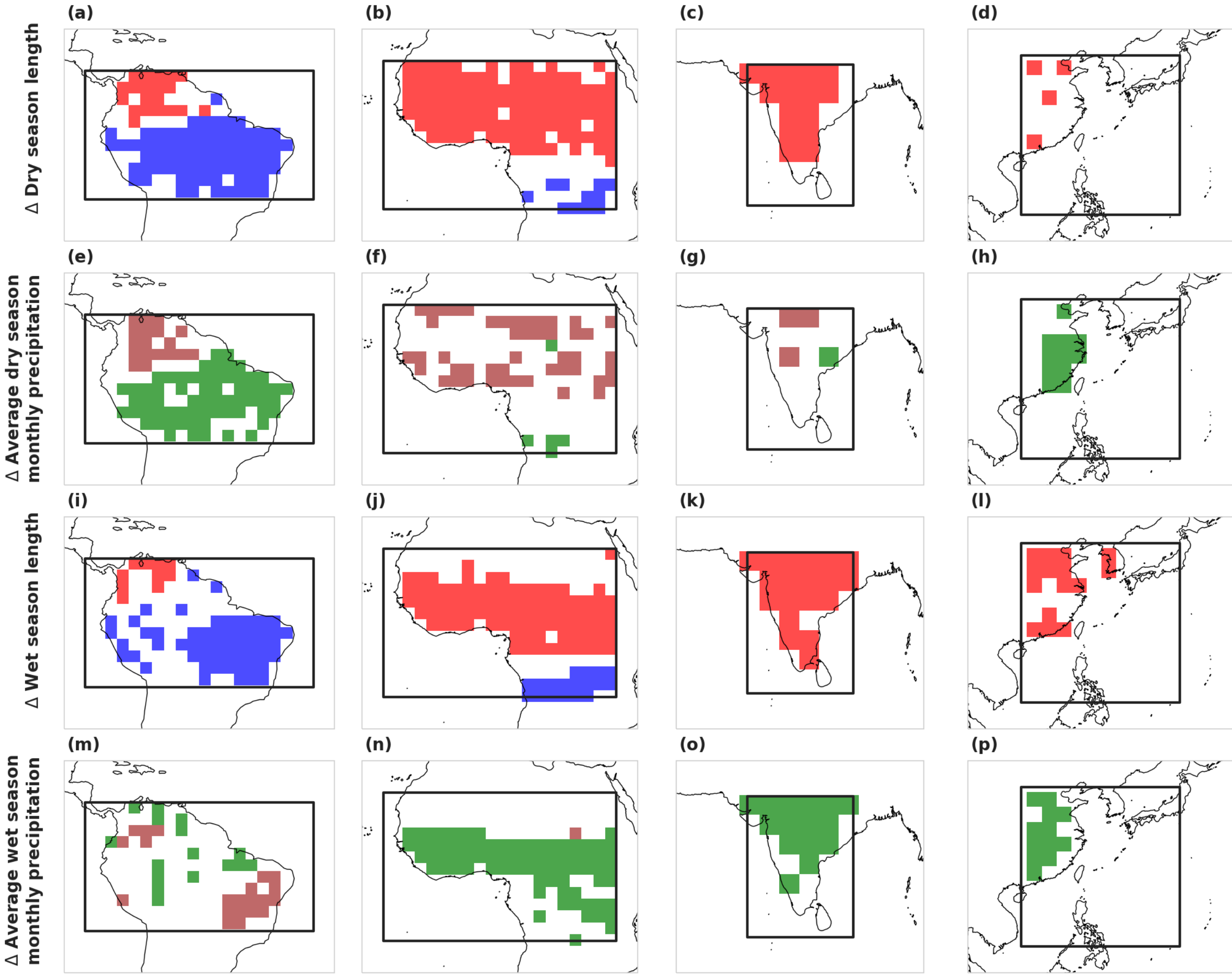

Figure S6. Coloured areas indicate regions of agreement of all four models for the dry and wet season length and precipitation change, as shown in Figure 5 for HadGEM. First row (a-d): blue (red) for shorter (longer) dry season. Second and fourth row (e-h and m-p): green (brown) for a wetter (drier) dry or wet season. Third row (i-l): blue (red) for longer (shorter) dry season. All models agree over the change in dry and wet season lengths over large regions of the SAM, WAM, EASM and ISM. There is less consistent agreement on the sign of the dry and wet season precipitation changes.

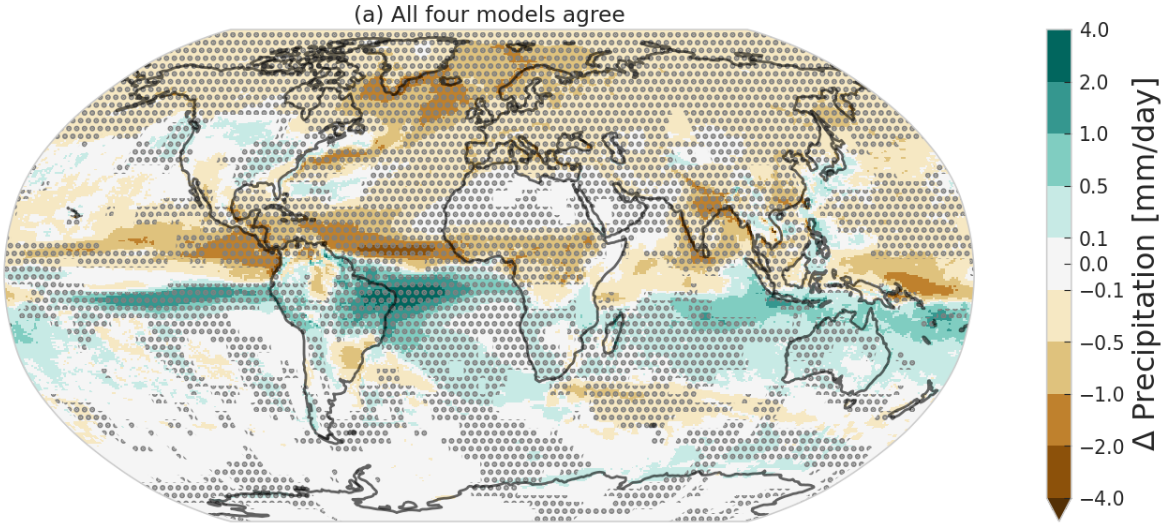

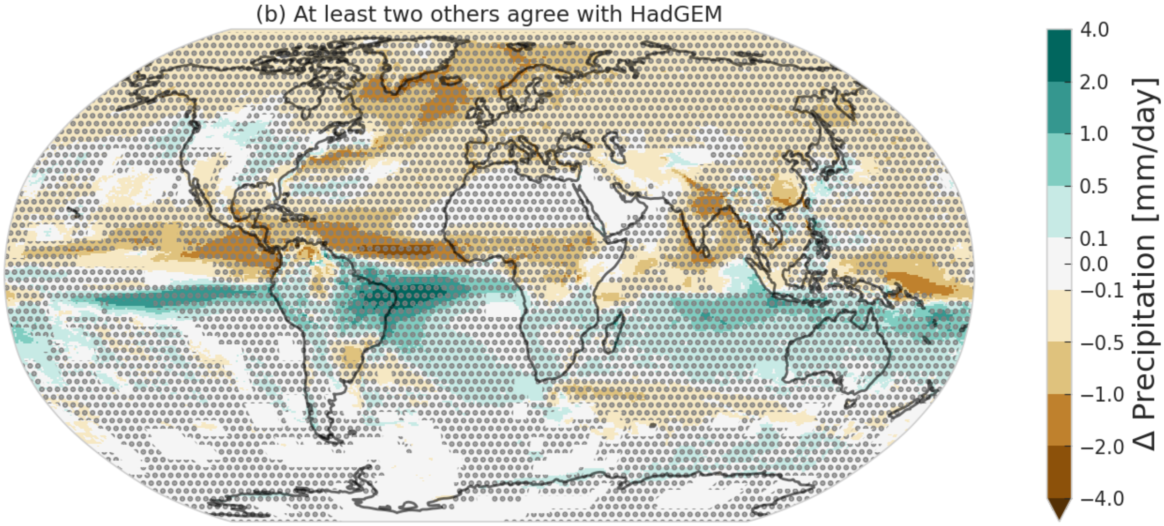

Figure S7. Comparison of the HadGEM precipitation anomaly (weak AMOC minus piControl) with the other model anomalies. In figure (a) the HadGEM precipitation anomaly is plotted and the stippling shows the regions where the sign of the precipitation anomaly in all four models is the same (all four are negative or all four are positive). Figure (b) is the same, but the stippling is in the areas where at least two other model precipitation anomaly signs agree with HadGEM. At least two other models agree with HadGEM over almost the complete monsoon regions, with the exception of the drying of the north-eastern SAM (which is only seen in HadGEM, see Figure 1).

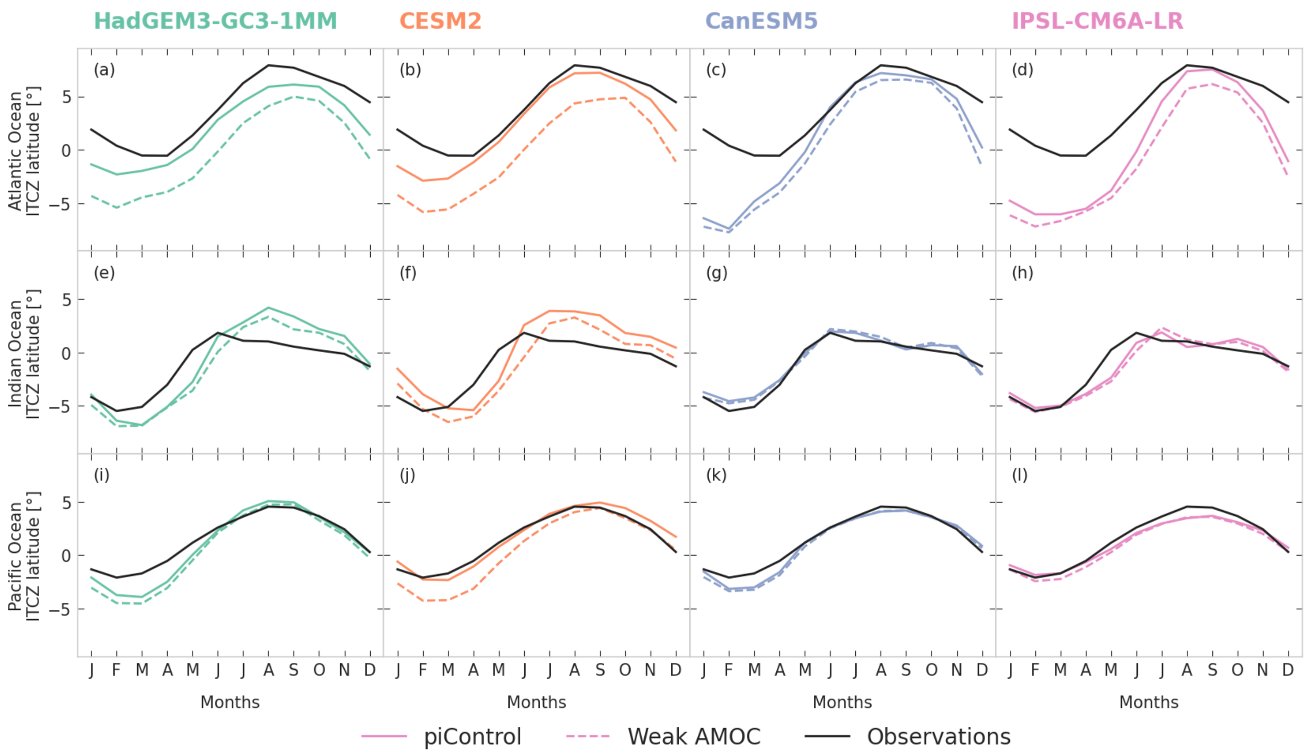

Figure S8. Monthly averages of the ITCZ latitude in the Atlantic (a-d), Indian (e-h) and Pacific oceans (i-l) (see methods). The coloured lines are the piControl (solid) and weak AMOC (dashed) runs. The solid black line shows the observations. All models are close to the observations in the Pacific ocean, and only HadGEM and CESM have a small bias in the Indian. As expected, for all models the Indian and Pacific ITCZs show only a small change after a collapse of the AMOC.

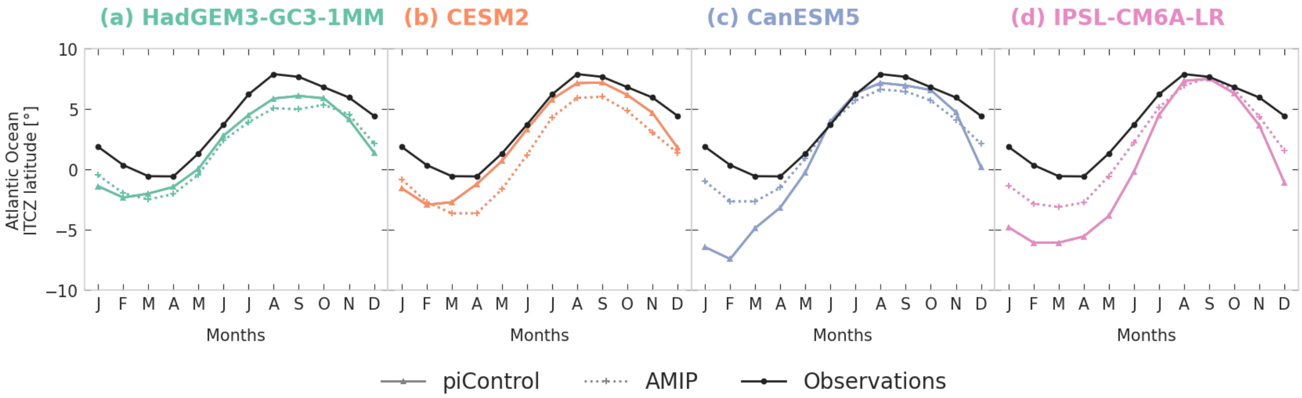

Figure S9. SST bias in the mean location of the Atlantic ITCZ for each month of the year for a. HadGEM3, b. CanESM, c. CESM, and d. IPSL The observational data is shown in black, the piControl model output in thick coloured lines and the AMIP model output in dotted coloured lines. For CanESM and IPSL the AMIP runs have a smaller ITCZ bias, suggesting that part of their Dec-Mar southwardly ITCZ bias is due to SST biases in the models.